Big bang nucleosynthesis constraints on hadronically and electromagnetically decaying relic neutral particles

Karsten Jedamzik

Laboratoire de Physique Mathémathique et Théorique, Université de Montpellier II, 34095 Montpellier Cedex 5, France
(Received 29 May 2006; published 8 November 2006)

Big bang nucleosynthesis in the presence of decaying relic neutral particles is examined in detail. All nonthermal processes important for the determination of light-element abundance yields of ^{2}H, ^{3}H, ^{3}He, ^{4}He, ^{6}Li, and ^{7}Li are coupled to the thermonuclear fusion reactions to obtain comparatively accurate results. Predicted light-element yields are compared to observationally inferred limits on primordial light-element abundances to infer constraints on the abundances and properties of relic decaying particles with decay times in the interval $0.01\ \mathrm{sec} \lesssim \tau_X \lesssim 10^{12}\ \mathrm{sec}$. Decaying particles are typically constrained at early times by ^{4}He or ^{2}H, at intermediate times by ^{6}Li, and at large times by the ^{3}He/^{2}H ratio. Constraints are shown for a large number of hadronic branching ratios and decaying particle masses and may be applied to constrain the evolution of the early universe.

DOI: 10.1103/PhysRevD.74.103509 PACS numbers: 98.80.Cq, 95.35.+d, 98.70.Vc

I. INTRODUCTION

The epoch of big bang nucleosynthesis (BBN) is one of the furthest reaching back probe of early cosmological conditions. It has thus been invaluable, for example, for the realization that baryonic matter contributes only a small fraction to the present critical density, thus providing independent evidence for the existence of dark matter, or that extensions of the standard model of particle physics which include further light degrees of freedom are observationally disfavored. Because of its usefulness, BBN has thus been analyzed in many variants (inhomogeneous BBN, BBN with leptonic chemical potentials, BBN with antimatter domains, BBN with decaying particles or evaporating primordial black holes, BBN with Brans-Dicke gravity, etc.; for reviews the reader is referred to Ref. [1]). These studies have been important for the realization that the Universe must have been fairly close during the BBN epoch (~ 1–10^4 sec) to that described by the standard model of BBN (SBBN). A SBBN scenario assumes a homogeneous baryonic plasma free of defects or decaying relics and with close-to-vanishing leptonic chemical potentials at constant baryon-to-entropy. With the recent accurate determination of the fractional contribution of baryons to the critical density $\Omega_b h^2 = 0.0223^{+0.0007}_{-0.0009}$ (h is the Hubble constant in units $100\ \mathrm{km\,s^{-1}\,Mpc^{-1}}$) by the Wilkinson Microwave Anisotropy Probe (WMAP) satellite mission [2], predicted primordial light elements in a SBBN scenario may be compared with those observationally inferred. This comparison is good when ^{2}H/H is considered, fair when ^{4}He, and inconclusive when ^{3}He is considered, but factor 2–3 discrepant in the case of ^{7}Li. It is not clear if this latter discrepancy is due to stellar ^{7}Li destruction effects, either in Pop II [3–6] stars where it is observed, or in a prior Pop III generation [7], or indeed due to a required modification of BBN, such as a population of decaying relics [8,9]. This discrepancy, however, is not the subject of the present paper.

The current study presents in detail analysis and results of BBN with decaying neutral particles. Such scenarios may easily emerge, for example, in supersymmetric extensions of the standard model, where relic gravitinos produced at high temperatures decay during BBN [10]. Similarly, when the gravitino is the lightest supersymmetric particle, next-to-lightest supersymmetric binos or sneutrinos may decay into gravitinos during or after BBN. Many such BBN studies have been presented before, from the pioneering works in the eighties [11–15] to improved and updated analysis in the nineties [16–18] up to very recent publications [8,19–21]. Nevertheless, except for Refs. [8,20,21], none of these works were able to properly treat the hadronic decay of a relic particle *during* BBN.

The purpose of this paper is twofold. It is intended to present a catalog of constraints on hadronically and electromagnetically decaying neutral particles over a wide range of decay times (10^{-2}–10^{12} sec) as well as hadronic branching ratios and relic particle masses. Prior studies have presented results only for a very small number of hadronic branching ratios. It should be noted that due to nonlinearities, either at smaller decay times ($\tau \lesssim 10^4$ sec) when thermal nuclear reactions still proceed or due to interference of electromagnetic destruction and hadronic production, for example, a simple interpolation between results at different hadronic branching ratios often leads to erroneous or inaccurate results. The second purpose of this study is to present the detailed analysis underlying the results presented in Refs. [8,9,22,23]. In general the philosophy in the analysis is to stay as close as possible to experimental data. Furthermore, a large number (93, cf. Table I) of processes are included, all those which the author believes to play a role at the more than a few percent level. Particular attention is given to an as accurate as

possible determination of the synthesized ^{6}Li in such scenarios. This is also of importance as ^{6}Li has been recently observed in surprisingly large abundance in about 10 Pop II stars [34] and is often a by-product of decaying [14,17] or annihilating [22] relic particles. Finally, it is noted that the present limits do not apply to decaying electrically charged relic particles with $\tau_X \gtrsim 100$ sec as in this case, the existence of bound states between nuclei and the relics may significantly change nuclear reaction rates [35].

The outline of the paper is as follows: In Sec. II a brief overview over the physics of BBN in the presence of electromagnetically and hadronically decaying particles is presented. Section III discusses observationally inferred primordial light-element abundances and derives the constraints on those as applied in the analysis. Section IV then presents the constraints which apply to the abundance of putative relic decaying particles, whereas conclusions are drawn in Sec. V. For the reader interested in details and for the benefit of the author, a number of appendices summarizes the analysis. This includes general considerations (Appendix A), the numerical procedure (Appendix B), employed kinematic relations (Appendix C), nonthermal electromagnetic interactions (Appendix D), nonthermal hadronic interactions (Appendix E), and the thermal nuclear reactions (Appendix F).

II. OVERVIEW OF THE PHYSICS OF BBN WITH DECAYING PARTICLES

This section gives a brief and schematic account of the modifications to BBN when energetic particles are injected due to, for example, the decay of relic particles. The decay channel of the relic determines the energy and nature of the injected primaries. A BBN calculation with decaying particles requires the detailed study of the thermalization of these primaries in the primordial plasma, as well as that of secondaries produced during the thermalization process. Since for one energetic primary several tens/hundreds of secondaries may be produced, such calculations are sometimes also referred to as cascade nucleosynthesis calculations. In addition, thermal nuclear reactions operative at early times ($\tau \lesssim 10^4$ sec) have to be followed. One distinguishes between primaries being either hadronic (nucleons, antinucleons, mesons), electromagnetic (photons, $e^{\pm}$), or inert (neutrinos or other weakly interacting particles). This distinction is useful as the thermalization of hadronically and electromagnetically interacting particles is very different and thus impacts the light-element yields in different ways. Both have nevertheless in common that over the whole range of decay times considered here (10^{-2}–10^{12} sec) thermalization occurs very rapidly on the Hubble scale. Redshifting of energetic particles has therefore not to be considered. In contrast, inert particles, such as neutrinos, have typically no further interactions with the plasma and thus also do not effect BBN yields. However, even neutrinos, if energetic enough ($\sim$ 100 GeV) and injected very early on ($\tau \sim 1$ sec) may not be regarded as inert (cf. Appendix E 1), but since their effects are typically subdominant compared to hadronically and electromagnetically interacting particles, they are not considered in the present study.

Hadronically interacting primaries may affect light-element yields in the whole above quoted decay time range. Charged mesons have an effect only during early times ($\tau \sim 10^{-1}$–10^{1} sec) due to charge-exchange reactions [15] (Rec. 34–43 Table I, Appendix E 1) with nucleons, converting mostly protons to neutrons and thereby increasing the ^{4}He abundance. At larger decay times their effects are negligible since they mostly decay before reacting with nucleons. At shorter decay times thermal weak interactions very quickly reestablish the SBBN neutron-to-proton ratio. Antinucleons may have an effect at all times, though their effect is the most pronounced during the time interval $\tau \sim 10^{-1}$–10^{2} sec (Appendix E 2). As they are more likely to annihilate on protons they also tend to increase the neutron-to-proton ratio. At times $\tau \gtrsim 200$ sec a significant fraction $Y_p \approx 0.25$ of all baryons are bound into helium nuclei. Annihilation of antinucleons on helium nuclei may leave ^{2}H, ^{3}H, and ^{3}He as secondaries [11]. However, this effect is subdominant as compared to the effects by injected nucleons.

Neutrons at $\tau \gtrsim 200$ sec and protons at $\tau \gtrsim 10^4$ sec thermalize to a substantial degree via nucleon-nucleon collisions (Rec. 48–73 Table I, Appendix E 3 and E 4) and nuclear spallation reactions (Rec. 74–83 Table I, Appendix E 5). This is because the competing processes for thermalization, magnetic moment scattering of neutrons off plasma $e^{\pm}$ (Rec. 3, Appendix D 1 c), Coulomb stopping of protons by plasma $e^{\pm}$ (Rec. 1, Appendix D 1 a), and Thomson scattering of protons on cosmic microwave background radiation (CMBR) photons (Rec. 2, Appendix D 1 b) loose their efficiency. This holds true except for very energetic nucleons as well as protons in the tens of MeV range and is due to ever decreasing numbers of $e^{\pm}$ and energy of CMBR photons. These results may be observed in Fig. 1. Each nucleon-nucleon scattering produces another energetic nucleon. The injection of an energetic 100 GeV nucleon may therefore lead to the production of several tens of 1 GeV nucleons. Their collective impact on the light-element yields via spallation of ^{4}He to produce ^{2}H, ^{3}H, and ^{3}He is far greater than that of a 100 GeV injected antinucleon [14]. The latter undergoes maximal 2–3 scattering before annihilating, with the respective probability of spallation of ^{4}He being comparatively small. The injection of nucleons is therefore always important. At early times this is due to an increase of the neutron density ($\tau \sim 1$–10^4 sec) leading to either an increased ^{4}He ($\tau \lesssim 200$ sec), increased ^{2}H ($\tau \sim 200$–10^4 sec), or decreased ^{7}Li ($\tau \sim 10^3$ sec) abundance. Somewhat later, and for the whole range of decay times considered here ($\tau \gtrsim 200$ sec) spallation of ^{4}He by ener-

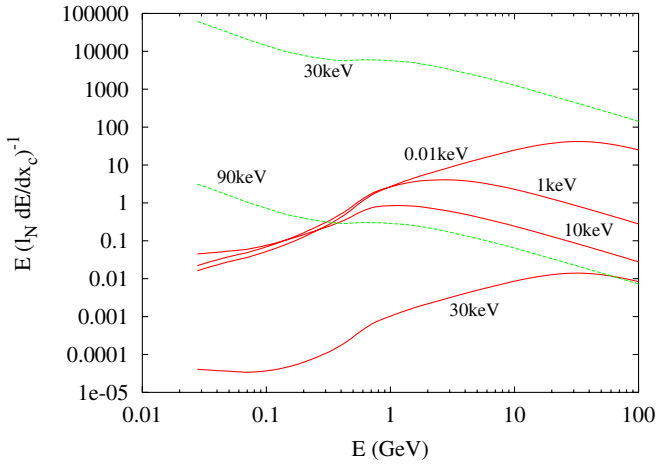

FIG. 1 (color online). The quantity $E(l_N|\mathrm{d}E/\mathrm{d}x|_c)^{-1}$ as a function of nucleon energy E, where l_N is the nucleon mean free path and $|\mathrm{d}E/\mathrm{d}x|_c$ is the nucleon energy loss per unit path length due to "continuous" energy losses such as multiple Coulomb scattering. When $E(l_N|\mathrm{d}E/\mathrm{d}x|_c)^{-1} \gtrsim 1$ nucleons predominantly lose energy due to nucleon-nucleon scattering and spallation processes, whereas in the opposite case nucleons lose their energy predominantly continuously via multiple electromagnetic scatterings on $e^{\pm}$ and photons [cf. Eq. (B1)]. Only in the former limit nuclear cascades occur. The quantity is shown for neutrons [dashed (green) line] at temperatures $T = 90$ and 30 keV and protons [solid (red) line] at temperatures $T = 30$, 10, 1 and 0.01 keV as labeled in the figure.

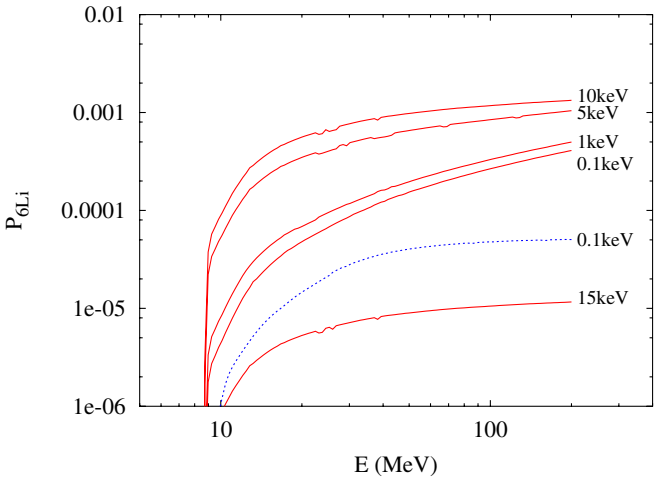

FIG. 2 (color online). Probability $P_{^6\mathrm{Li}}$ of energetic ^{3}H nuclei [solid (red) line] and energetic ^{3}He [dotted (blue) line] of initial energy E to fuse on ambient ^{4}He nuclei to form ^{6}Li via the reactions $^3\mathrm{H}(\alpha, n)^6\mathrm{Li}$ and $^3\mathrm{He}(\alpha, p)^6\mathrm{Li}$, respectively. The figure shows this probability for ^{3}H nuclei at temperatures $T = 5$, 10, 5, 1 and 0.1 keV and for ^{3}He nuclei at temperature $T = 0.1$ keV, respectively. Survival of the freshly formed ^{6}Li nuclei against thermal nuclear reactions is also taken into account as evident by the comparatively low $P_{^6\mathrm{Li}}$ at $T = 15$ keV. The figure illustrates that $P_{^6\mathrm{Li}}$ dramatically increases at $T \sim 5 - 10$ keV due to a decrease of the efficiency of Coulomb stopping in this narrow temperature interval (see text).

getic nucleons and their secondaries yields large amounts of ^{2}H, ^{3}H, and ^{3}He. These trends may be seen in Fig. 3. As ^{4}He spallation processes by neutrons in the time range $\tau \sim 200$–10^4 sec are by far more efficient than those by protons, inelastic nucleon-nucleon reactions (Rec. 52–73, Appendix E 4) which preferentially convert protons to neutrons are also important for accurate BBN yield predictions.

The spallation of ^{4}He to form ^{3}H and ^{3}He is also important as it may lead to the synthesis of ^{6}Li [14] (cf. Appendix E 6). The mass three nuclei ^{3}H and ^{3}He emerge energetic from these reactions with typical energies around 10 MeV. They may thus participate in the nonthermal fusions reactions 85–86 to form ^{6}Li. The formation of ^{7}Li by those energetic mass three nuclei, as well as by energetic ^{4}He resulting from elastic nucleon-^{4}He collisions (Rec. 87–88) is by far less important. Energetic mass three nuclei to the largest part lose their energy efficiently via Coulomb stopping. However, even the comparatively small fraction $\sim 10^{-4}$ (cf. Fig. 2) which fuses may yield an observationally important ^{6}Li abundance. The freshly fused ^{6}Li may survive thermal nuclear

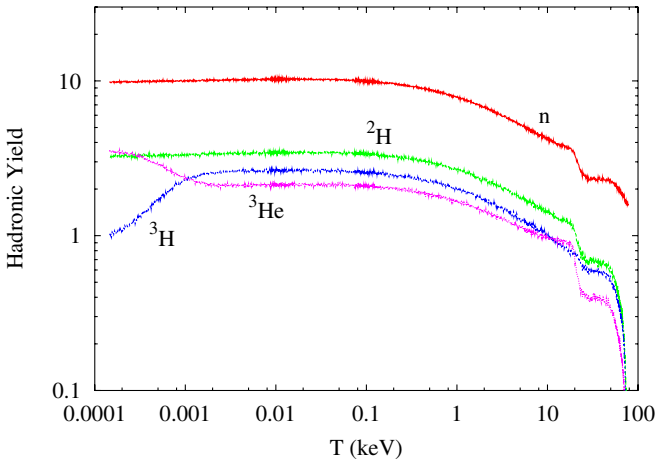

FIG. 3 (color online). Yields of (from top to bottom) neutrons (red), deuterium nuclei (green), tritium nuclei (blue), and ^{3}He nuclei (magenta) as a function of cosmic temperature T per hadronically decaying particle $X \rightarrow q\bar{q}$ of mass $M_x = 1$ TeV, where q denotes a quark. Note that initially after hadronization of the q-$\bar{q}$ state on average only 1.56 neutrons result. The remainder of the created neutrons at lower temperatures $T \lesssim 90$ keV are resulting from the thermalization of the injected neutrons (and protons) due to inelastic nucleon-nucleon scattering processes and ^{4}He spallation processes. Similarly, all the ^{2}H, ^{3}H, and ^{3}He nuclei are due to ^{4}He spallation processes and np nonthermal fusion reactions (for ^{2}H) induced by the thermalization of the injected energetic nucleons. The figure does note include the electromagnetic yields (cf. Fig. 4) due to photodisintegration which is inevitable even for a hadronic decay since approximately 45% of the rest mass energy of the decaying particle is converted into energetic γ rays and energetic $e^{\pm}$ after hadronization and pion decays.

reactions only above $\tau \gtrsim 10^4$ sec. A particularity in the Coulomb stopping (cf. Appendix D 1 a) which renders it very much less efficient for nuclei with velocities below the thermal electron velocity, which is the case for $\sim$10 MeV mass three nuclei at $\tau \sim 10^4$ sec, increases the ^{6}Li production efficiency around this time by a factor of 10. As explained in Appendix E 6, ^{6}Li yields due to energetic mass three nuclei produced by ^{4}He spallation are somewhat uncertain and may well be some tens of percents higher. The uncertainty is due to an incomplete knowledge of the high-energy tail of produced mass three nuclei which may well include a backward scattering peak. The present study is therefore conservative in estimating ^{6}Li yields.

Electromagnetically interacting particles may impact BBN yields only at comparatively large decay times ($\tau \gtrsim 10^5$ sec). This is due to energetic photons and $e^\pm$ interacting efficiently with CMBR photons (cf. Appendix D 2). γ rays rapidly pair produce on CMBR photons (Rec. 4) and electrons inverse Compton scatter (Rec. 5). Comparatively long-lived against further interactions are only γ-rays of energies below the $e^\pm$ pair production threshold. This threshold is at $E \approx 2.2$ MeV at $\tau \sim 10^5$ sec and increases continuously as the CMBR temperature drops reaching $E \approx 19.8$ MeV at $\tau \sim 10^7$ sec. These latter energies are the thresholds for photodisintegration of ^{2}H and ^{4}He, respectively. Once γ rays have dropped below the pair production threshold their interactions close to the threshold are dominated by scattering of CMBR photons (Appendix D 2 d), and further below the threshold by Bether-Heitler pair production (Appendix D 2 a) and Compton scattering (Appendix D 2 c). A substantial though small fraction $f \sim 0.01$ may photodisintegrate either ^{4}He or ^{2}H [12]. The reader is referred to Figs. 4 and 5 for typical light-element production and destruction factors

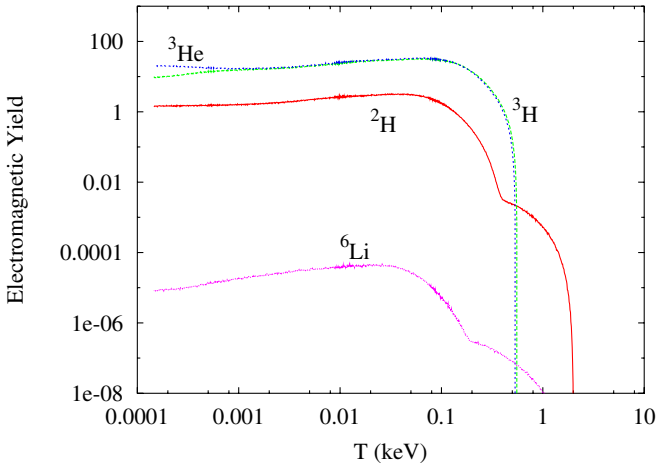

FIG. 4 (color online). Yields of (from top to bottom) ^{3}He (blue), ^{3}H (green), ^{2}H (red), and ^{6}Li (magenta) nuclei per TeV of electromagnetically interacting energy injected (in form of energetic γ rays and energetic $e^\pm$) due to photodisintegration reactions (^{2}H, ^{3}H, ^{3}He, and ^{6}Li) and fusion reactions (^{6}Li) as a function of cosmic temperature.

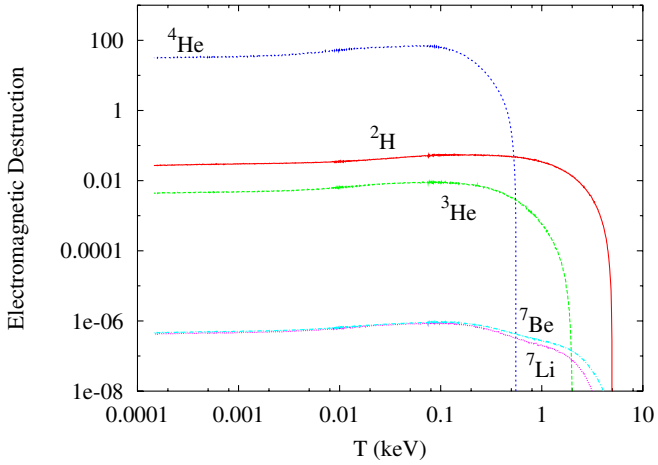

FIG. 5 (color online). Number of destroyed (from top to bottom) ^{4}He (blue), ^{2}H (red), ^{3}He (green), and ^{7}Li (magenta) (^{7}Be light blue) nuclei per TeV of electromagnetically interacting energy injected into the primordial plasma at temperature T. For the purpose of illustration we have taken the ^{7}Li and ^{7}Be abundances equal at $^7\mathrm{Li/H} = {}^7\mathrm{Be/H} \approx 4.34 \times 10^{-10}$. In reality it is the sum of both isotopes which is synthesized at $(^7\mathrm{Li} + {}^7\mathrm{Be})/\mathrm{H} \approx 4.34 \times 10^{-10}$ in a SBBN scenario at $\Omega_b h^2 \approx 0.02233$ with ^{7}Be being converted to ^{7}Li by electron capture at cosmic temperatures $T \approx 0.1$–1 keV.

during electromagnetic decays. When ^{4}He photodisintegration becomes important ($\tau \gtrsim 10^7$ sec), photodisintegration of ^{2}H is a subdominant effect as more ^{2}H is produced in the relatively larger numbers of ^{4}He nuclei which are photodisintegrated. Energetic ^{3}H and ^{3}He produced in large numbers during the ^{4}He photodisintegration may lead via nonthermal fusion reactions to ^{6}Li [17], similar to the energetic mass three nuclei produced in ^{4}He spallation during hadronic decays. To a less important degree ^{6}Li also may be created by direct photodisintegration of ^{7}Li and ^{7}Be.

Thus, the effects of injection of electromagnetically interacting particles on BBN yields are due to photodisintegration and are only operative at comparatively late times ($\tau \gtrsim 10^5$ sec). A much simplifying aspect of BBN with electromagnetically decaying particles is the fact that results almost always only depend on the total amount of electromagnetically interacting energy, rather than the energy and nature of the injected primary. This is due to the number of cascade photons and electrons being so large that asymptotically the same state is reached, independent of the initial state. Finally it is noted that hadronic decays (such as $X \rightarrow q\bar{q}$, with q a quark) generically also lead to the injection of electromagnetically interacting primaries, as, for example, due to π^0's which decay into two photons.

III. OBSERVATIONAL LIMITS ON THE PRIMORDIAL ABUNDANCES

The following provides a compilation of the observational limits on primordial abundances adopted in the present

analysis. For more detail on observations and interpretations, the reader is either referred to the original literature or reviews on BBN nucleosynthesis (cf. [36,37]).

A. ^{4}He

The primordial ^{4}He abundance is inferred from observations of hydrogen- and helium-emission lines in extragalactic low-metallicity HII regions. The two most recent observers' determinations yield $Y_p \approx 0.2421 \pm 0.0021$ [38] and $Y_p \approx 0.239 \pm 0.002$ [39]. Nevertheless, somewhat smaller $Y_p \approx 0.2345$ or larger $Y_p \approx 0.2443$ determinations by the same authors, but determined from (partially) different data sets, also have been cited. The estimates are significantly below the SBBN Y_p prediction at the WMAPIII baryon density. However, the quoted error bars are purely statistical in nature and only some of the many possible systematic errors could be estimated. Systematic errors include underlying stellar absorption, ionization corrections, temperature fluctuations, and collisional excitation. Recent reanalysis of the original data by an independent group [40] has led to a significantly revised $Y_p \approx 0.249 \pm 0.009$ estimate, including a substantial increase of the error bars. Nevertheless, even this latter study does not include a study of the majority of systematic uncertainties, such that its utility is somewhat questionable. Many of these systematic uncertainties would lead again to a decrease of the inferred Y_p. In a conservative spirit, however, the present analysis utilizes the upper limit as quoted above

$$Y_p < 0.258. \tag{1}$$

A lower limit on Y_p is not considered as usually of no use for deriving limits on relic decaying particles.

B. ^{2}H

The most accurate method for an observational determination of the primordial ^{2}H/H ratio is believed to be due to observations of low-metallicity quasar absorption line systems (QALS). Such gaseous systems, on the line of sight between a high redshift quasar and the observer, produce absorption lines in the continuous spectrum of the quasar at the redshifted wavelength of the Lyman-α ^{2}H and ^{1}H positions, respectively. If the QALS has a simple velocity structure, the depths of the absorption troughs may be used to infer the ^{2}H/H ratio. As observations focus on systems at very low metallicity, the assumption is typically that only very little stellar ^{2}H destruction has occurred, and that the determined abundance may be directly compared to the predicted BBN ^{2}H/H ratio. When the currently six best determinations [41] are averaged, one obtains a QALS-inferred primordial ^{2}H/H abundance of $^2\mathrm{H/H} \approx 2.4 \pm 0.4 \times 10^{-5}$ [36]. This value compares favorably to that predicted by a SBBN scenario at the WMAPIII baryonic density. Nevertheless, caution has to be applied as the intrinsic dispersion between individual central values of ^{2}H/H determinations is much larger than most of the quoted error bars for individual QALS. Thus, the highest individual 2-σ upper limit and the lowest individual 2-σ lower limit of all six systems span a range

$$1.2 \times 10^{-5} \lesssim {}^2\mathrm{H/H} \lesssim 5.3 \times 10^{-5}, \tag{2}$$

much larger than the above quoted error bar. Furthermore, a systematic trend of decreasing ^{2}H/H with increasing column density N_H of the QALS may be found indicating the existence of possible systematic errors. Attempting to remain on the conservative side, the above range is adopted in the analysis for an acceptable ^{2}H/H abundance. Conservatism may be in order not only because a recent proposal of a very active stellar Pop III population, which could potentially reduce the primordial ^{2}H/H ratio in certain (high N_H) systems without much trace of associated iron or silicon production [7].

C. ^{3}He/^{2}H

Precise observational determinations of ^{3}He/H ratios are only possible within our galaxy. Since our galaxy is chemically evolved, it is difficult to make a straightforward connection to the primordial ^{3}He/H abundance. Since ^{3}He, in fact, is known to be destroyed in some stars, but produced in others, observed ^{3}He/H ratios may also only with difficulty be utilized to obtain an upper or lower limit on the primordial ^{3}He/H. This is in contrast to the ^{3}He/^{2}H ratio. ^{2}H is known to be always destroyed in stars (in fact is burned into ^{3}He), whereas ^{3}He is either destroyed or produced. The cosmic ^{3}He/^{2}H ratio may therefore only increase with time. Thus a determination of this ratio in any environment, even chemically evolved, may be taken as an upper limit on the primordial ^{3}He/^{2}H ratio [42]. From a combination of solar wind observations and the planetary gas component of meteorites and Jupiter, it is possible to infer the $^3\mathrm{He/H} \approx 1.66 \pm 0.05 \times 10^{-5}$ and $^2\mathrm{H/H} \approx 1.94 \pm 0.39 \times 10^{-5}$ ratios at the time of solar system formation independently [43]. Employing the 2-σ upper end of the ^{3}He abundance and the 2-σ lower end of the ^{2}H abundance, when may derive a conservative constraint of

$$^3\mathrm{He}/^2\mathrm{H} < 1.52, \tag{3}$$

for the primordial ^{3}He/^{2}H ratio.

D. ^{7}Li

For a long time it has been known that the ^{7}Li/H ratio in the atmospheres of low-metallicity PopII stars is essentially constant with metallicity (the Spite plateau) with deduced central values on the plateau falling in the range $1.23 \times 10^{-10} \lesssim {}^7\mathrm{Li/H} \lesssim 1.73 \times 10^{-10}$ [44]. As this value is traditionally interpreted to be close to the primordial ^{7}Li/H ratio, a factor 2–3 discrepancy between the SBBN predicted primordial ^{7}Li/H at the WMAPIII baryon density (usually in excess of 4×10^{-10}) and that inferred from

the stars on the Spite plateau is apparent. This situation has neither been changed by a large number of reevaluations of the ^{7}Li/H abundance of the Spite plateau, nor convincingly shown to be solved by stellar depletion of ^{7}Li. As the ^{7}Li isotope is not very important in constraining relic decaying particles (rather, it may resolve the problem), the reader is referred elsewhere for discussion of this problem (e.g. [7,9,36]). The present analysis adopts only a lower limit on the primordial ^{7}Li/H

$$^7\mathrm{Li/H} > 0.85 \times 10^{-10}, \tag{4}$$

chosen by the 95% confidence level lower limit as derived by Ref. [45].

E. ^{6}Li

The isotope of ^{6}Li can be particularly useful in deriving constraints on relic decaying particles [17]. Recently, the number of claimed preliminary detections of ^{6}Li/^{7}Li ratios in low-metallicity Pop II stars has multiplied by a large factor [34] (cf. to Ref. [46] for the few former detections) falling in the range $0.03 \lesssim {}^6\mathrm{Li}/{}^7\mathrm{Li} \lesssim 0.07$ with average ^{6}Li/^{7}Li ≈ 0.042 and with no star having ^{6}Li/^{7}Li in excess of 0.1. The origin of this ^{6}Li is unknown. Concerning a limit on the primordial ^{6}Li abundance, the situation is somewhat problematic. This is particularly so, since the predicted SBBN ^{7}Li is in excess of that observed. If this latter fact is after all explained by stellar ^{7}Li destruction, ^{6}Li would also be destroyed. In the best case (destroying as little as possible ^{6}Li), both the ^{6}Li and ^{7}Li abundances would be destroyed by the same factor, with their ratio, nevertheless, staying constant. In this case one may adopt

$$^6\mathrm{Li}/^7\mathrm{Li} \lesssim 0.1 \tag{5}$$

as upper limit. This would correspond to a primordial ^{6}Li abundance $^6\mathrm{Li/H} \lesssim 4.34 \times 10^{-11}$ (given that the SBBN prediction is 4.34×10^{-10} in the present analysis, cf. Appendix F) already much in excess of the 2-σ upper limit of $^6\mathrm{Li/H} < 1.47 \times 10^{-11}$ in the well-studied star HD84937. However, calculations of ^{6}Li and ^{7}Li destruction in stars generally predict more ^{6}Li destruction than ^{7}Li destruction, since ^{6}Li is more fragile than ^{7}Li. In Ref. [3] which studied ^{7}Li depletion in rotating stars a correlation between the amount of ^{7}Li and ^{6}Li destruction was obtained, with, for example, factor 2(4) reduction of the ^{6}Li/^{7}Li ratio occurred for factor 1.6(2.5) reduction of the ^{7}Li abundance. When the (fine-tuned) models by Ref. [4] are taken, designed to explain a larger amount of ^{7}Li destruction without spoiling the flatness of the Spite plateau (when plotted against stellar temperature), a factor 1.6(2.5) of ^{7}Li destruction implies a factor 1.25(15.8) reduction in the ^{6}Li/^{7}Li ratio. Particularly the last destruction factor would render the ^{6}Li isotope not anymore as useful in deriving limits on decaying particles. Nevertheless, in the spirit of a conservative study we will also adopt

$$^6\mathrm{Li}/^7\mathrm{Li} \lesssim 0.66 \qquad \text{conservative}, \tag{6}$$

as a second more conservative limit. Here this value derives by taking the average observed ^{6}Li/^{7}Li ratio of 0.042 and multiplying it by the ^{6}Li/^{7}Li destruction factor of 15.8. This is done with the understanding that any models which violate Eq. (5) but not Eq. (6) should be flagged as potentially being ruled out. On the other hand, such models, if not violating other observational constraints, could also explain the origin of the observed ^{6}Li (cf. Ref. [8,9]).

IV. CONSTRAINTS ON RELIC DECAYING PARTICLES

In this section conservative constraints on the abundance of putative relic decaying neutral particles in the early Universe are presented. The number density n_X of an early produced semistable particle species X with decay width $\Gamma_X = 1/\tau_X$ follows the equation

$$\frac{\mathrm{d}n_X}{\mathrm{d}t} = -3Hn_X - \frac{n_X}{\tau_X}, \tag{7}$$

where t is cosmic time and H is the Hubble constant. Here the first term on the right-hand side describes dilution due to cosmic expansion, whereas the second term represents the particle decay. Results are presented for a large number of different hadronic branching ratios B_h of the particle X. In particular, it is assumed that a fraction B_h of all decays are hadronic and a fraction $1 - B_h$ are electromagnetic. During hadronic decays the primaries injected into the plasma are assumed to be a quark-antiquark pair of total energy M_X and total momentum zero in the cosmic rest frame. The hadronization of the q-$\bar{q}$ fluxtube is followed with aid of the code PYTHIA, resulting in numerous nucleons, mesons, $e^{\pm}$, and γ rays injected into the plasma. Note that for large M_X, as considered here, the spectrum of the resulting post-hadronization particles is virtually independent of the type of initial quark injected. As already stated in Sec. II, for sufficiently massive particles X the effects of electromagnetic decays on BBN yields depends only on the total energy $E_{e,\gamma}$ in $e^{\pm}$ and γ rays injected into the plasma. For electromagnetic decays $E^{\mathrm{EM}}_{e,\gamma} = M_X$ is thus assumed with no injection of nucleons or mesons. Hadronic decays are also associated with the release of energetic electromagnetically interacting particles. Following results from PYTHIA $E^{\mathrm{H}}_{e,\gamma} = 0.45M_X$ is taken. Finally, it is noted that only baryon number conserving decays are considered.

In Figs. 6–8 constraints on the abundance of $M_X = 1$ TeV relic decaying particles for hadronic branching ratios $B_h = 1$, $B_h = 3.333 \times 10^{-2}$, and $B_h = 10^{-3}$, respectively, are shown. The colored (shaded) regions are excluded, with different colors (shades) corresponding to constraints derived from different light elements, as indicated in the figure captions. It is evident that the most stringent constraints derive from an overproduction of

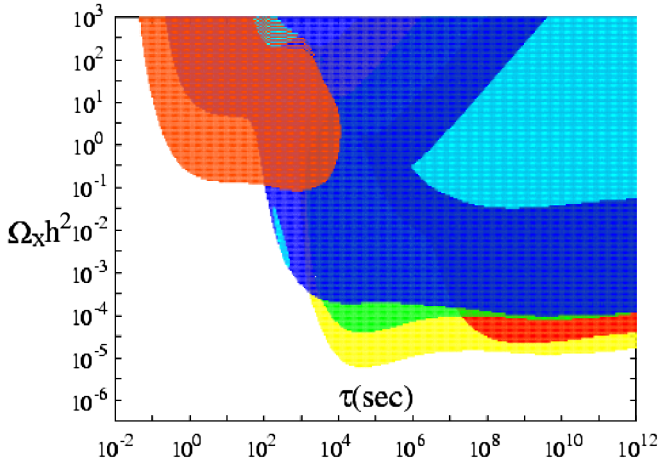

FIG. 6 (color online). Conservative BBN constraints on the abundance of relic decaying neutral particles as a function of their life time for an $M_x = 1$ TeV particle with hadronic branching ratio $B_h = 1$. Limits are given on the contribution the decaying particles would have made to the present critical density, $\Omega_X h^2$ (with h the Hubble parameter), if they would have not decayed. For a conversion to constraints on, for example $M_X n_X/n_\gamma$ the reader is referred to Appendix A. The shaded regions are excluded and correspond to the constraints imposed by the observationally inferred upper limit on ^{4}He (orange) [Eq. (1)], upper limit on ^{2}H (blue) [Eq. (2)], upper limit on ^{3}He/^{2}H (red) [Eq. (3)], and lower limit on ^{7}Li (light blue) [Eq. (4)]. Conservative constraints derived from ^{6}Li/^{7}Li [Eq. (6)] are shown by the green region. The region indicated by yellow violates the less conservative ^{6}Li/^{7}Li [Eq. (5)] constraint but should not be considered ruled out. Rather, this region may be cosmologically interesting as a putative source of ^{6}Li in low-metallicity stars by relic decaying particles.

^{4}He at early times $\tau_X \lesssim 10^2$ sec, an overproduction of ^{2}H in the decay time interval 10^2 sec $\lesssim \tau_X \lesssim 10^3$ sec, an overproduction of ^{6}Li in the decay time interval 10^3 sec $\lesssim \tau_X \lesssim 10^7$ sec, and an overproduction of the ^{3}He/^{2}H ratio

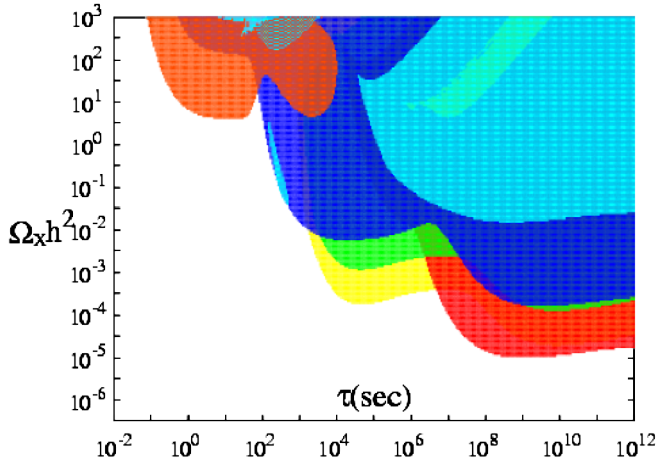

FIG. 7 (color online). As Fig. 6 but for hadronic branching ratio $B_h = 3.333 \times 10^{-2}$.

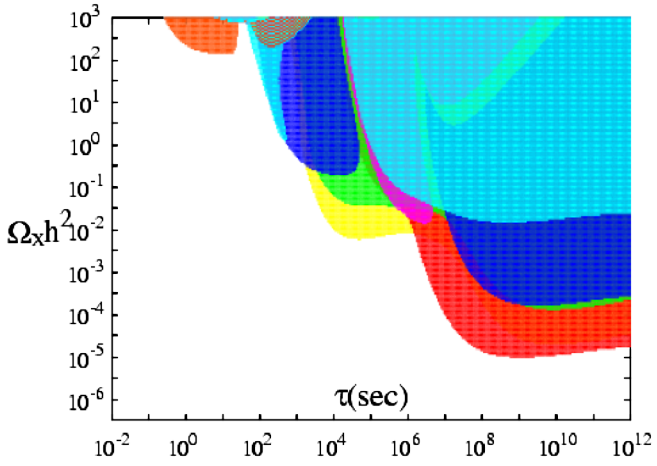

FIG. 8 (color online). As Fig. 6 but for hadronic branching ratio $B_h = 10^{-3}$. The region excluded by the lower limit on ^{2}H/H [Eq. (2)] (magenta) is also apparent.

for large decay times $\tau_X \gtrsim 10^7$ sec. The lightly shaded (yellow) area in the figures corresponds to elevated ^{6}Li production in the range $0.1 \lesssim {}^6\text{Li}/{}^7\text{Li} \lesssim 0.66$ and should currently not be considered ruled out. Though in excess of the observationally inferred ^{6}Li/^{7}Li abundance ratio in low-metallicity stars, it is conceivable that some of the produced ^{6}Li has been destroyed in low-metallicity stars. The reader is referred to Sec. III E for details. In contrast, as the source of the unexpected large abundance of ^{6}Li in

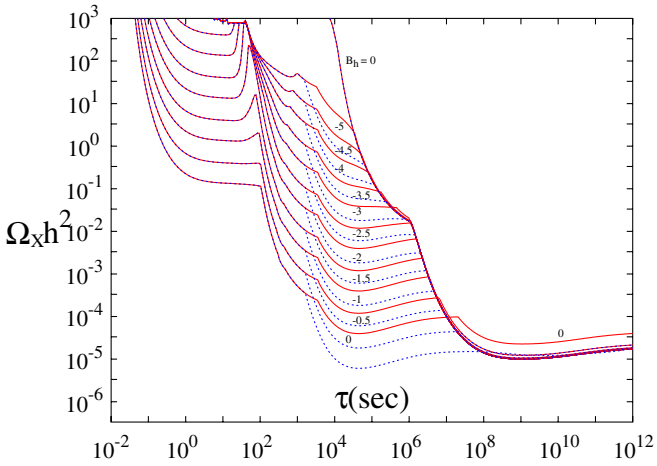

FIG. 9 (color online). Constraints on the abundance of decaying neutral particles as a function of life time for an $M_X = 1$ TeV particle with varying hadronic branching ratios. Constraints are shown for hadronic branching ratios (from bottom to top) $\log_{10} B_h = 0, -0.5, -1, -1.5, -2, -2.5, -3, -3.5, -4, -4.5$, and -5, respectively, as labeled. The case $B_h = 0$ is also shown. The labels always correspond to the solid (red) line above it. For each B_h the region above this solid (red) line is ruled out when conservative constraints are applied [i.e. Eqs. (1)–(4) and (6)]. When the ^{6}Li/^{7}Li constraint Eq. (6) is replaced by the less conservative Eq. (5) the dotted (blue) constraint lines result. These dotted lines coincide for small and large τ_X with the solid (red) lines.

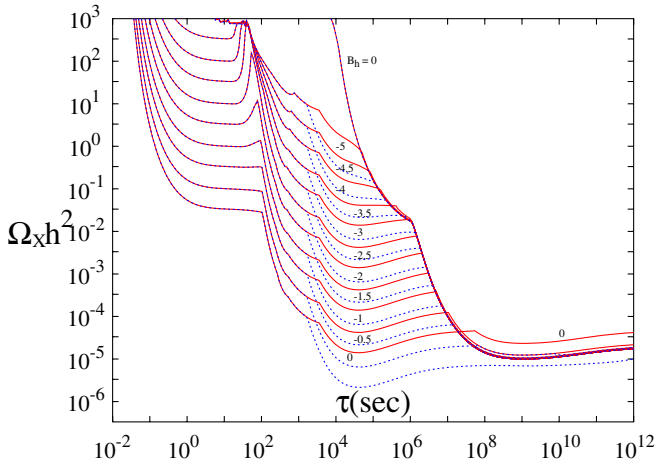

FIG. 10 (color online). As Fig. 9 but for $M_X = 100$ GeV.

low-metallicity stars is unknown, the yellow region may be considered as cosmologically interesting [8,9].

In Figs. 9 and 10 constraints on the abundance of relic decaying particles for a large number of hadronic branching ratios and two different particle masses, $M_X = 100$ GeV and $M_X = 1$ TeV, are shown. The region above the solid (red) lines for each particular B_h are excluded. The figure also shows by the dotted (blue) lines how the constraints would change if one were to replace the observationally inferred limit on $^6\mathrm{Li}/^7\mathrm{Li}$ in Eq. (6) by the less conservative constraint Eq. (5). However, as argued above, the latter constraint should currently not be applied.

V. CONCLUSIONS

BBN is a powerful probe of the conditions in the early universe and may severely limit the putative existence of relic decaying particles. In this paper, the effects of electromagnetically and hadronically decaying particles on the BBN light-element synthesis of ^{2}H, ^{3}He, ^{4}He, ^{6}Li, and ^{7}Li have been considered in detail. All processes which the author believes to play a role at the 10% level have been included. These include nucleon-nucleon elastic and inelastic scatterings, nucleon-antinucleon annihilation, spallation of ^{4}He by energetic nucleons, fusion reactions of ^{3}H and ^{3}He on ^{4}He-nuclei, mesonic charge exchange, Coulomb- and magnetic-moment scattering, Thomson scattering, Bethe-Heitler pair production, photon-photon scattering, (inverse) Compton scattering, and photodisintegration of light nuclei, among others. The analysis attempts to stay as close as possible to existing experimental data. A number of expressions, as, for example, the Coulomb stopping power of comparatively slow nuclei have been newly evaluated. All these nonthermal reactions are coupled to the thermonuclear fusion reactions known to be of importance during BBN. Results of such complete calculations have been first presented in Refs. [8,20] and particularly, Ref. [21], nevertheless, only for a limited number of decaying particle properties.

Predicted light-element yields are compared to observationally inferred limits on primordial light-element abundances to infer accurate and conservative limits on electromagnetically and hadronically decaying particles in the early universe. Constraints on the abundance of such decaying particles are shown for a large number of hadronic branching ratios and particles masses. This was necessary to obtain comparatively accurate limits as a simple extrapolation between the results of only two hadronic branching ratios may yield to erroneous or inaccurate results. The results in this paper may be used to further constrain the evolution of the very early universe.

ACKNOWLEDGMENTS

I acknowledge useful exchanges with D. Arndt, M. Asplund, A. Blinov, J. Bystricky, R. Cyburt, M. Chadeyeva, P. Descouvemont, E. Keihanen, H.-P. Morsch, K. Olive, N. Prantzos, O. Richard, and E. Vangioni-Flam.

APPENDIX A: GENERAL CONSIDERATIONS

For the computation of light-element abundance yields in the presence of decaying or annihilating relic particles during or after BBN one has to essentially treat the thermalization process of energetic nucleons, antinucleons, and γ rays. These latter particles result as primaries from the decay/annihilation process. Their thermalization occurs due to a host of processes discussed in detail in Appendices D and E. At the same time, thermal nuclear reactions of the thermal baryonic component may play a role at high temperatures $T \gtrsim 10$ keV. In general, the problem simplifies considerably due to two facts: (a) thermalization may be treated as an instantaneous process on the Hubble time scale and (b) interactions between two nonthermal nucleons/nuclei are improbable. Given a typical proton density $n_p \approx 1.6 \times 10^{16}/\mathrm{cm}^3 (T/10\ \mathrm{keV})^3$ and a typical nucleon (nuclei)-nucleon interaction cross section of 30 mb and 300 mb at nucleon (nuclei) kinetic energy $E_k \approx 1$ GeV and 10 MeV, respectively, one finds a typical scattering time $\tau_N \approx 0.07\ \mathrm{sec}(T/10\ \mathrm{keV})^{-3}$ which is approximately constant with kinetic energy. This may be compared to the Hubble time $\tau_H \approx 1.4 \times 10^4 (T/10\ \mathrm{keV})^{-2}$ sec to yield a ratio $10\tau_N/\tau_H \approx 5 \times 10^{-5}(T/10\ \mathrm{keV})^{-1}$ where it is approximated that it takes around ten scatterings for the complete thermalization of a nucleon. It is seen that only at very low temperatures $T \lesssim 0.1$ eV thermalization may not be regarded instantaneous on the Hubble scale. Because of the short survival times of energetic nucleons (nuclei) only for excessively large ratios of nonthermalized-to-thermalised nucleons $\Omega_{\mathrm{non-thermal}}/\Omega_b \sim 10^4 (T/10\ \mathrm{keV})$ interactions between two nonthermalized nucleons become important. For such large $\Omega_{\mathrm{non-thermal}}$, however, BBN (almost) always fails badly in predicting the observationally inferred pri-

TABLE I. Nonthermal reactions included in the present analysis.

No.	Reaction	Channel	Ref.	No.	Reaction	Channel	Ref.
1	$p + e^{\pm} \rightarrow$ elastic	Coulomb	Appendix D 1 a	48	$p + p \rightarrow$	elastic	[25,26], Appendix E 3
2	$p(N) + \gamma_{\mathrm{CMBR}} \rightarrow$	Thomson	Appendix D 1 b	49	$p + {}^4\mathrm{He} \rightarrow$	elastic	[25], Appendix E 3
3	$n + e^{\pm} \rightarrow$	magnetic moment	Appendix D 1 c	50	$n + p \rightarrow$	elastic	[25,26], Appendix E 3
4	$\gamma + \gamma_{\mathrm{CMBR}} \rightarrow$	$e^- + e^+$	Appendix D 2	51	$n + {}^4\mathrm{He} \rightarrow$	elastic	[25], Appendix E 3
5	$e^{\pm} + \gamma_{\mathrm{CMBR}} \rightarrow$	inverse Compton	Appendix D 2 and D 2 b	52	$p + p \rightarrow$	$p + p + \pi^0$	[24], Appendix E 4
6	$\gamma + p({}^4\mathrm{He}) \rightarrow$	$p({}^4\mathrm{He}) + e^- + e^+$	Appendix D 2 a	53		$n + p + \pi^+$	[24,27], Appendix E 4
7	$\gamma + e^- \rightarrow$	Compton	Appendix D 2 c	54		${}^2\mathrm{H} + \pi^+$	[24,27], Appendix E 4
8	$\gamma + \gamma_{\mathrm{CMBR}} \rightarrow$	$\gamma + \gamma$	Appendix D 2 d	55		$p + p + \pi^+\pi^-$	[24], Appendix E 4
				56		${}^2\mathrm{H} + \pi^+\pi^0$	[24], Appendix E 4
9	$\gamma + {}^2\mathrm{H} \rightarrow$	$p + n$	[28]	57		${}^2\mathrm{H} + 2\pi^+\pi^-$	[24], Appendix E 4
10	$\gamma + {}^3\mathrm{H} \rightarrow$	${}^2\mathrm{H} + n$	[28]	58		$p + p + \pi^+\pi^-\pi^0$	[24], Appendix E 4
11		$2n + p$	[28]	59		$n + p + 2\pi^+\pi^-$	[24], Appendix E 4
12	$\gamma + {}^3\mathrm{He} \rightarrow$	${}^2\mathrm{H} + p$	[28]	60		$p + p + 2\pi^0 + (\pi^0 s)$	[24,27], Appendix E 4
13		$2p + n$	[28]	61		$n + n + 2\pi^+ + (\pi^0 s)$	[24], Appendix E 4
14	$\gamma + {}^4\mathrm{He} \rightarrow$	${}^3\mathrm{H} + p$	[28]	62		$n + p + \pi^+ + (\pi^0 s)$	[24,27], Appendix E 4
15		${}^3\mathrm{He} + n$	[28,29]	63	$n + p \rightarrow$	$p + n + \pi^0 + (\pi^0 s)$	[24], Appendix E 4
16		${}^2\mathrm{H} + {}^2\mathrm{H}$	[28]	64		${}^2\mathrm{H} + \pi^0 + (\pi^0 s)$	[24], Appendix E 4
17		${}^2\mathrm{H} + n + p$	[28]	65		$p + p + \pi^-$	[24], Appendix E 4
18	$\gamma + {}^6\mathrm{Li} \rightarrow$	${}^4\mathrm{He} + n + p$	[28,30]	66		$n + n + \pi^+$	[24], Appendix E 4
19		${}^3\mathrm{A} + X$	[28]	67		$n + p + \pi^-\pi^+$	[24,27], Appendix E 4
20	$\gamma + {}^7\mathrm{Li} \rightarrow$	${}^4\mathrm{He} + {}^3\mathrm{H}$	[28,31]	68		$p + p + \pi^-\pi^0 + (\pi^0 s)$	[24], Appendix E 4
21		${}^6\mathrm{Li} + n$	[28]	69		${}^2\mathrm{H} + \pi^-\pi^+$	[24], Appendix E 4
22		${}^4\mathrm{He} + 2n + p$	[28]	70		$n + n + \pi^+ + (\pi^0 s)$	[24,27], Appendix E 4
23		${}^4\mathrm{He} + {}^2\mathrm{H} + n$	Appendix D 3	71		$n + p + 2\pi^-2\pi^+$	[24], Appendix E 4
24		${}^6\mathrm{He} + p \rightarrow {}^6\mathrm{Li} + p$	Appendix D 3	72		$n + p + \pi^-\pi^+\pi^0$	[24], Appendix E 4
25		$2{}^3\mathrm{H} + p$	Appendix D 3	73		$p + p + 2\pi^-\pi^+$	[24], Appendix E 4
26		${}^3\mathrm{H} + {}^3\mathrm{He} + n$	Appendix D 3				
27	$\gamma + {}^7\mathrm{Be} \rightarrow$	${}^4\mathrm{He} + {}^3\mathrm{He}$	[28,32]	74	$p + {}^4\mathrm{He} \rightarrow$	${}^3\mathrm{H} + 2p + (\pi s)$	Appendix E 5 and E 6.
28		${}^6\mathrm{Li} + p$	[28]	75		${}^3\mathrm{He} + n + p + (\pi s)$	Appendix E 5 and E 6.
29		${}^4\mathrm{He} + 2p + n$	[28]	76		${}^2\mathrm{H} + 2p + n + (\pi s)$	Appendix E 5
30		${}^4\mathrm{He} + {}^2\mathrm{H} + p$	Appendix D 3	77		${}^3\mathrm{He} + {}^2\mathrm{H}$	Appendix E 5 and E 6.
31		${}^6\mathrm{Be} + n \rightarrow {}^4\mathrm{He} + 2p + n$	Appendix D 3	78		${}^2\mathrm{H} + {}^2\mathrm{H} + p + (\pi s)$	Appendix E 5
32		${}^{32}\mathrm{He} + n$	Appendix D 3	79	$n + {}^4\mathrm{He} \rightarrow$	${}^3\mathrm{He} + 2n + (\pi s)$	Appendix E 5 and E 6.
33		${}^3\mathrm{H} + {}^3\mathrm{He} + p$	Appendix D 3	80		${}^3\mathrm{H} + n + p + (\pi s)$	Appendix E 5 and E 6.
				81		${}^2\mathrm{H} + 2n + p + (\pi s)$	Appendix E 5
34	$\pi^+ + n \rightarrow$	$\pi^0(\gamma) + p$	[15], Appendix E 1	82		${}^3\mathrm{H} + {}^2\mathrm{H}$	Appendix E 5 and E 6.
35	$\pi^- + p \rightarrow$	$\pi^0(\gamma) + n$	[15], Appendix E 1	83		${}^2\mathrm{H} + {}^2\mathrm{H} + n + (\pi s)$	Appendix E 5
36	$K^- + n \rightarrow$	$p + X$	[15], Appendix E 1	84	$p + {}^6\mathrm{Li} \rightarrow$	${}^3\mathrm{He} + {}^4\mathrm{He}$	Appendix E 5
37		$n + X$	[15], Appendix E 1				
38	$K^- + p \rightarrow$	$n + X$	[15], Appendix E 1	85	${}^3\mathrm{H} + {}^4\mathrm{He} \rightarrow$	${}^6\mathrm{Li} + n$	Appendix E 6
39		$p + X$	[15], Appendix E 1	86	${}^3\mathrm{He} + {}^4\mathrm{He} \rightarrow$	${}^6\mathrm{Li} + p$	Appendix E 6
40	$K_L + n \rightarrow$	$p + X$	[15], Appendix E 1	87	${}^4\mathrm{He} + {}^4\mathrm{He} \rightarrow$	${}^6\mathrm{Li} + {}^2\mathrm{H}({}^6\mathrm{Li} + p + n)$	Appendix E 6
41		$n + X$	[15], Appendix E 1	88		${}^7\mathrm{Li} + p({}^7\mathrm{Be} + n)$	Appendix E 6
42	$K_L + p \rightarrow$	$n + X$	[15], Appendix E 1				
43		$p + X$	[15], Appendix E 1	89	${}^3\mathrm{He} + p \rightarrow$	elastic	Appendix E 6
				90	${}^3\mathrm{H} + p \rightarrow$	${}^3\mathrm{He} + n$	Appendix E 6
44	$\bar{p} + p \rightarrow$	π's	[15], Appendix E 2	91	${}^3\mathrm{H} + p \rightarrow$	elastic	Appendix E 6
45	$\bar{n} + p \rightarrow$	π's	[15], Appendix E 2	92	${}^3\mathrm{H} \rightarrow$	${}^3\mathrm{He} + e^- + \bar{\nu}_e$	[33], Appendix E 6
46	$\bar{p} + n \rightarrow$	π's	[15], Appendix E 2	93	${}^7\mathrm{Be} + e^- \rightarrow$	${}^7\mathrm{Li} + \nu_e$	[33]
47	$\bar{n} + n \rightarrow$	π's	[15], Appendix E 2				

mordial abundances, such that such interactions may be neglected.

Abundance yields due to decaying particles may be often understood as the product of individual factors. For example, for the production of ^{6}Li nuclei by the fusion reactions 85 and 86, induced by nonthermal mass three nuclei, one may schematically write the final number of produced ^{6}Li nuclei $\Delta N_{^6\mathrm{Li}}$, produced during a certain cosmic expansion interval $\mathrm{d}\ln a$

$$\Delta N_{^6\mathrm{Li}} = \int \mathrm{d}N_{^6\mathrm{Li}} = \int \mathrm{d}\ln a \left(\frac{\mathrm{dDecays}}{\mathrm{d}\ln R}\right)\left(\frac{n_{p,n}}{\mathrm{Decay}}\right)\left(\frac{n_3}{n_{p,n}}\right)\left(\frac{n_6}{n_3}\right), \quad \text{(A1)}$$

where a denotes the cosmic scale factor. Here the integrand is composed of the number of relic particle decays per logarithmic scale factor interval, times the number of energetic nucleons produced per decay, times the number of energetic ^{3}H and ^{3}He produced during the thermalization of a nucleon, times the fraction of ^{3}H and ^{3}He nuclei which fuse to form ^{6}Li. Similarly, there are contributions from photodisintegration not shown in Eq. (A1). The present analysis treats in detail the third and fourth factors, pertaining to thermalization. For example, the last factor in the integrand (n_6/n_3) may be seen in Fig. 2 for various cosmic temperatures. The second factor is given by an assumed initial post decay state (e.g. $q\bar{q}$ an energetic quark-antiquark fluxtube at an assumed energy) in combination with the results of a hadronization code, such as PYTHIA, which computes the number and energy of produced (anti)nucleons, mesons, and γ rays after hadronization of the initial $q\bar{q}$ fluxtube. This factor $(n_{p,n}/\mathrm{Decay})$ convolved with $(n_3/n_{p,n})$ may be seen in Fig. 3 (cf. also to Fig. 4 for a similar convolution due to photodisintegration). Finally, the first factor is given by the assumed abundance and life time of the putative relic.

All figures in the main text limit $\Omega_X h^2$, the contribution of the decaying particle density to the present critical density Ω_X if the particle were not decaying. Here h is the present Hubble constant in units of 100 km s^{-1} Mpc^{-1}. Other studies often present limits on the number of X particles per photon times M_X, the mass of the X particle, or the number of X particles per radiation entropy times M_X. The conversion factors between these quantities are given by $\xi_1 = n_X M_X/n_\gamma = 2.5784 \times 10^{-8}$ GeV$\Omega_X h^2$ and $\xi_2 = n_X M_X/s = 3.6639 \times 10^{-9}$ GeV$\Omega_X h^2$.

APPENDIX B: NUMERICAL MONTE CARLO PROCEDURE

The present analysis utilizes a Monte Carlo approach to the problem. At each time step of the order of 10^4 nonthermal nucleons and 6×10^3 γ rays are injected into the thermal plasma. Here there initial energies are randomly drawn, in the case of nucleons, from a kinetic energy distribution function generated by PYTHIA, and in the case of photons, from the distribution function given in Eq. (D8). Mesons, which to a large part thermalize before interacting, are injected in their number ratios predicted by PYTHIA. The subsequent evolution of each nucleon is followed by a Monte Carlo (random probabilistic) sequence of events. Energy losses of nucleons are determined by a competition between nuclear scattering (spallation) processes (Appendix E 3–E 5), in which a nucleon may lose a good part of its energy, and continuous energy losses, such as Coulomb stopping, Thomson scattering, and magnetic moment scattering (Appendix D 1). The probability of survival of a nucleon (nuclei) k against nuclear scattering while it loses continuously energy between energy E_i and E_f is given by

$$P_k(E_i \rightarrow E_f) = \exp\left(- \int_{E_f}^{E_i} \frac{\mathrm{d}E}{l_N^k(E)|\mathrm{d}E/\mathrm{d}x|_c} \right), \qquad \text{(B1)}$$

where $|\mathrm{d}E/\mathrm{d}x|_c$ is the energy-dependent continuous energy loss per unit path length and $1/l_N^k = \sum_i \sigma_{ki\rightarrow\ldots} n_i$ is the inverse of the nucleon (nuclei) mean free path against nuclear scattering. This probability distribution is mapped in the analysis by utilizing random numbers. Further, the evolution of any secondary energetic nucleons due to nuclear scattering is followed as well. The thermalization of nucleons is followed down to energies below which inelastic processes are not anymore possible. The remainder of the thermalization occurs quickly through elastic processes and does not further influence the BBN yields. In Fig. 1 an approximation to the integrand in Eq. (B1) may be seen for protons and neutrons at various cosmic temperatures.

Photons are treated in a similar way. Each injected photon and the by it produced secondaries are followed in a Monte Carlo way until all photons have dropped below the lowest photodisintegration threshold. The number of nuclei (nucleons) A per decaying particle X produced due to all γ rays created as a consequence of the decay of X are computed via

$$\frac{N_A}{\mathrm{Decay}} = \left(\sum_i \frac{\mathrm{d}N(E_\gamma)}{\mathrm{d}E_\gamma^i} \Delta E_\gamma^i \right) \left(\sum_B n_B \sum_j \sigma_{B\gamma\rightarrow A\ldots} c\tau_j(E_\gamma^j) - n_A \sum_j \sigma_{A\gamma\rightarrow C\ldots} c\tau_j(E_\gamma^j) \right). \qquad \text{(B2)}$$

Here the sum over index i runs over the energy spectrum of the initial (after CMBR cascade) γ ray spectrum, σ are photodisintegration cross sections, c is the speed of light, and $\tau_j(E_\gamma^j)$ are γ ray survival times against the processes discussed in Appendices D 2 a, D 2 c, D 2 d, and D 3. The sums over i and j are different due to the inclusion of secondary photons. In particular, a photon with initial energy E_γ^i may produce secondary photons j due to the processes described in Appendix D 2. The sum over j thus includes all γ's, primary and secondary, tertiary, ... as long as they are above the photodisintegration threshold. Individual survival times are generated by a Monte Carlo and the γ ray survival probability $P_\gamma(E_\gamma) = \exp(\tau c/l_\gamma(E_\gamma))$, with $l_\gamma(E_\gamma)$ the γ mean free path. Finally, it is noted that for accuracy reasons the initial first-generation photon spectrum Eq. (D8) is sampled by an equal amount of photons above and below the photodisintegration threshold for ^{4}He. This was necessary as otherwise much larger ($\gg 6 \times 10^3$) numbers of photons would have to be followed in order to obtain accurate result.

APPENDIX C: KINEMATIC RELATIONS

For the convenience of the author, this appendix presents some kinematic relations required to convert cross section

data presented in terms of center-of-mass (CM) quantities to cross section data in the laboratory (L) frame of reference. For the energy gain of particle 2 (initially at rest) in elastic $2 \rightarrow 2$ scattering, and given the scattering angle in the CM frame, one finds

$$\Delta E_{L,2} = \gamma_{v_{\rm CM}}^2 v_{\rm CM}^2 M_2 (1 - \cos\Theta_{\rm CM}), \tag{C1}$$

where $v_{\rm CM} = p_L^1/(M_2 + M_1 + E_{L,\rm kin}^1)$, $E_{\rm CM,2} = \gamma_{v_{\rm CM}} M_2$, and $|p_{\rm CM}| = v_{\rm CM}\gamma_{v_{\rm CM}} M_2$. (Note that $|p_{\rm CM}|$ is invariant during elastic scattering.) Concerning inelastic endothermic $2 \rightarrow 2$ scattering reactions $1 + 2 \rightarrow 3 + 4$ with 2 initially at rest (e.g. reactions 77, 82, 85–88), the threshold in the laboratory system is given by $E_L^1 = \Delta m(1 + m_1/m_2)$ with $\Delta m = (m_3 + m_4 - m_1 - m_2)$, the mass differences. During inelastic $2 \rightarrow 2$ scattering with particle 2 initially at rest, $|p_{\rm CM}|$ is not anymore invariant due to conversion of kinetic energy to rest energy. Utilizing the above given (before scattering) $v_{\rm CM}$, $|p_{\rm CM}|$ relations, one may solve the implicit equation $E_{\rm CM}^1 + E_{\rm CM}^2 = E_{\rm CM}^3 + E_{\rm CM}^4$ for $p'_{\rm CM}$, with $E_{\rm CM}^3$, and $E_{\rm CM}^4$ containing the after scattering modified $p'_{\rm CM}$. Provided one has $\Theta_{\rm CM}$, the CM scattering angle, the laboratory energy of particles 3 and 4 are determined by $E_L^3 = \gamma_{v_{\rm CM}}(E_{\rm CM}^3 + v_{\rm CM}|p'_{\rm CM}|\cos\Theta_{\rm CM})$ and similarly for particle 4 with $v_{\rm CM} \rightarrow -v_{\rm CM}$.

APPENDIX D: NONTHERMAL ELECTROMAGNETIC INTERACTIONS

1. Electromagnetic stopping of nonthermal nucleons

a. Coulomb interactions

Stopping of charged protons and nuclei by Coulomb scatterings off ambient electrons (and positrons) as well as excitation of collective plasma modes (involving a larger number of electrons) is particularly important. In the early universe single particle scatterings off electrons and positrons dominate. Since many of these occur with only small momentum transfer (i.e. small-angle scatterings) the process may be regarded as a continuous energy loss for protons and nuclei. Following Jackson [47] and my own calculations, the energy loss per unit path length traveled may be found:

$$\frac{{\rm d}E_C}{{\rm d}x} = \frac{Z^2\alpha}{v^2}\omega_p^2\left(\ln\left[\frac{0.76v}{\omega_p b}\right] + \frac{1}{2}v^2\right), \tag{D1}$$

where

$$\omega_p^2 = \frac{4\pi n_{e^\pm}\alpha}{m_e} \tag{D2}$$

is the square of the plasma frequency, and

$$b = \max\left[\frac{Z\alpha}{\gamma m_e v^2}, \frac{1}{\gamma m_e v}\right]. \tag{D3}$$

In these expressions Z, v, and γ refer to electric charge number, velocity, and Gamma factor of the nuclei, respectively, m_e is the electron mass, α the fine structure constant, and $n_{e^\pm}$ the total number density of electrons and positrons. This latter is given by

$$n_{e^\pm} \approx (n_{e,\rm net}^2 + n_{e,\rm pair}^2)^{1/2} \quad \text{with}$$
$$n_{e,\rm pair} = \frac{1}{2}\left(\frac{2}{\pi}\right)^{3/2}(m_e T)^{3/2} e^{-m_e/T}\left(1 + \frac{15T}{8m_e}\right), \tag{D4}$$

where T is cosmic temperature. Here $n_{e,\rm net}$ refers to the electrons needed for charge neutrality of the Universe. Equation (D4) is only accurate in the $T/m_e \ll 1$ limit. Note that the second term in Eq. (D1) derives from the magnetic moment scattering contribution of the electron absent in the Rutherford scattering cross section but present in the correct Mott scattering cross section. Note also that, in contrast to the findings of Ref. [15], it is found that Eq. (D1) is also valid in the extremely relativistic limit up to $\gamma \lesssim M_p/m_e$, where M_p is the proton mass. Nevertheless, an important modification to Eq. (D1) occurs for small nuclear velocities and large temperatures when the nuclear velocity v falls below the typical thermal electron velocity v_e. In this case the Coulomb stopping power decreases by a factor v_e/v^3 [15], a very larger factor 500 for, example, tritium nuclei of 10 MeV kinetic energy at a temperature of $T = 20$ keV. In order to obtain an accurate result for the stopping length in this regime an adequate thermal average over the electron velocity distribution has to be performed, as Coulomb stopping is dominated by Coulomb collisions off slow electrons. After a lengthy calculation the author finds

$$\frac{{\rm d}E_C}{{\rm d}x} = \frac{4\pi(Z\alpha)^2}{m_e v} n_{e^\pm}\left({\rm erf}(y)\left[\frac{\Lambda}{v}\left(1 - \frac{T}{2m_e}\right) + \frac{1}{2}\left(v - \frac{1}{v}\frac{T}{m_e}\right)\right] - \frac{2}{\sqrt{\pi}}e^{-y^2}\frac{y}{v} \times \left(\Lambda\left(1 - \frac{T}{2m_e} + \frac{v^2}{8} + \frac{m_e}{T}\frac{v^4}{8}\right) - \frac{T}{2m_e}\right]\right) \tag{D5}$$

for the Coulomb stopping which includes a thermal average over a Maxwell-Boltzmann distribution of electron (positron) velocities. Here $y = \sqrt{m_e v^2/2T}$ such that for $y \gg 1$ one recovers the result Eq. (D1) where the velocities of all electrons are below that of the nucleus. The term Λ in Eq. (D5) denoted the logarithm in Eq. (D1). Note that in Eq. (D5) an expansion has been performed to lowest nontrivial order in the small parameters v and $\sqrt{T/m_e}$, where both have been regarded to be of the same order.

b. Thomson scattering

Energetic protons may lose energy to the CMBR by Thomson scattering, a process which is particularly efficient at high CMBR temperature. Because of the large number of CMBR photons, many scatterings are involved and the energy loss of protons due to Thomson drag may also be treated as a continuous energy loss. Following

Reno and Seckel [15] and our own calculations, one finds

$$\frac{dE_{\rm Th}}{dx} = \frac{32\pi}{9}\frac{\pi^2 T^4}{15}\frac{\alpha^2}{M_p^2}\gamma_p^2 v_p Z^4, \quad \text{(D6)}$$

for the energy loss per unit length where α and T are fine structure constant and CMBR temperature, M_p the proton mass, γ_p and v_p its gamma factor and velocity, and Z its electric charge. Note that Eq. (D6) is applicable for protons of arbitrary relativity.

c. Magnetic moment scattering

Neutrons may lose energy due to scattering off electrons and positrons by virtue of their anomalous magnetic moment. This process is only important at higher temperature $T \sim 50$ keV due to the larger numbers of $e^{\pm}$. By aid of a calculation employing the relevant interaction amplitude one may find

$$\frac{dE_n}{dx} = \frac{3\pi\alpha^2\kappa^2 m_e}{M_n^2}\gamma_n^2 v_n^2 n_{e^{\pm}}, \quad \text{(D7)}$$

where $\kappa = -1.91$ is the anomalous magnetic dipole moment and all other notation is as before. Equation (D7) applies for nonrelativistic as well as relativistic neutrons.

2. Electromagnetic cascades induced by γ rays and charged particles

The injection of energetic electromagnetically interacting particles in the early universe leads to a cascade on the CMBR with γ rays pair producing ($\gamma + \gamma_{\rm CMBR} \rightarrow e^+ + e^-$) and the produced electrons (positrons) inverse Compton scattering ($e^{\pm} + \gamma_{\rm CMBR} \rightarrow e^{\pm} + \gamma$) off the CMBR photons [48–52]. This cascade is very rapid due to the large number of CMBR photons. Only when γ-ray energies have fallen below that for pair production $E_\gamma < m_e^2/E_{\rm CMBR}$ interactions on protons and nuclei become important. The spectrum of these "breakout" photons below the pair production threshold depends essentially only on the total electromagnetically interacting energy E_0 injected above E_C. It has been found to be well approximated by [51,52]

$$\frac{dN_\gamma}{dE_\gamma} = \begin{cases} K_0\left(\frac{E_\gamma}{E_X}\right)^{-1.5} & \text{for } E_\gamma < E_X \\ K_0\left(\frac{E_\gamma}{E_X}\right)^{-2} & \text{for } E_C \geq E_\gamma \geq E_X \end{cases}, \quad \text{(D8)}$$

where $K_0 = E_0/(E_X^2[2 + \ln(E_C/E_X)])$ is a normalization constant such that the total energy in γ rays below E_C equals the total energy E_0 injected. Following the analysis of Ref. [52], a value of $E_C \approx m_e^2/22T$ is employed in the present analysis with $E_X \approx 0.03E_C$ [49]. These values are very close to those ($E_C \approx m_e^2/23.6T$ and $E_X \approx 0.0264E_C$) advocated by Ref. [51]. Subsequent interactions of these breakout photons include photon-photon scattering ($\gamma + \gamma_{\rm CMBR} \rightarrow \gamma + \gamma$) mainly redistributing the energy of energetic γ rays right below energy E_C, Bethe-Heitler pair production ($\gamma + p(^4{\rm He}) \rightarrow p(^4{\rm He}) + e^- + e^+$), Compton scattering ($\gamma + e^- \rightarrow \gamma + e^-$) off thermal electrons, with the produced energetic e^- inverse Compton scattering to generate further low-energy γ rays, as well as nuclear photodisintegration. All these processes are included in the analysis and their detailed treatment is described below.

a. Bethe-Heitler pair production

The cross section for $e^{\pm}$ pair production by γ rays of energy E_γ scattering off protons and helium nuclei at rest is given by

$$\sigma_{\rm BH} \approx \frac{3}{8}\frac{\alpha}{\pi}\sigma_{\rm Th}\left(\frac{28}{9}\ln\left[\frac{2E_\gamma}{m_e}\right] - \frac{218}{27}\right)Z^2, \quad \text{(D9)}$$

where $\sigma_{\rm Th}$, α, m_e, and Z are Thomson cross section, fine structure constant, electron mass, and nuclear electric charge, respectively. The expression is valid in the regime $1 \ll E_\gamma/m_e \ll \alpha^{-1}Z^{-1/3}$. For energies in the range $2m_e < E_\gamma < 4$ MeV, the cross section is roughly approximated as constant at the value of Eq. (D9) at $E_\gamma = 4$ MeV. The energy of the produced e^- (e^+) is approximated by a flat probability distribution within the range $[m_e, E_\gamma - 2m_e]$ with the antiparticle e^+ (e^-) carrying the remainder of E_γ.

b. Inverse compton scattering

Electrons and protons produced during the dominant Bethe-Heitler process may upscatter CMBR photons to γ-ray energies by inverse Compton scattering. As these γ-rays may later photodistintegrate nuclei, a fairly accurate treatment of inverse Compton scattering is required. Here the exact inverse Compton scattering rate is unimportant since it is always large compared to the Hubble expansion. For the cumulative probability distribution that an e^- (e^+) of energy $E_e = \gamma_e m_e$ upscatters a CMBR photon to energy $E_\gamma = 4\gamma_e^2 Tx$, where T is CMBR temperature, one may find

$$P_{ic} \approx e^{-x}\left(1 + \frac{1}{4}x - \frac{1}{4}x^2\right) + \Gamma(0, x)\left(\frac{1}{4}x^3 - \frac{3}{4}x\right), \quad \text{(D10)}$$

with

$$\Gamma(0, x) = \int_x^\infty dy e^{-y}/y \quad \text{(D11)}$$

is an incomplete Gamma function. Note that for the evaluation of Eq. (D10), the approximation that the $e^{\pm}$ are ultrarelativistic, i.e. $\gamma_e \gg 1$, and that the scattering process occurs in the Thomson regime, i.e. $12\gamma_e T/m_e \ll 1$, have been made. These approximations are appropriate since only ultrarelativistic $e^{\pm}$ may produce γ rays by inverse Compton scattering on the CMBR which are energetic enough to photodisintegrate nuclei, and since $e^{\pm}$ produced during Bethe-Heitler pair production are not energetic

enough for the inverse Compton scattering to proceed in the Klein-Nishina limit. Furthermore for the derivation of Eq. (D10) the Einstein-Bose occupation number $(e^{-E_\gamma} - 1)^{-1}$ has been approximated by $\xi(3)e^{-E_\gamma}$ with $\xi(3) \approx 1.2021$ such that the total number of CMBR photons remains the same. The approximation was required to find a closed form for P_{ic}. By comparison to an accurate numerical evaluation, one finds that the approximation is typically good to within 3%–10%. Lastly one finds for the average scattered CMBR photon energy a value of $\langle E_\gamma \rangle = \gamma_e^2 \langle E_{\rm CMBR} \rangle$ with $\langle E_{\rm CMBR} \rangle \approx 2.701T$ the average CMBR photon energy.

c. Compton scattering

The cross section for γ rays of energy E_γ scattering off electrons at rest in the Klein-Nishina limit $E_\gamma \gg m_e$ is given by [53]

$$\sigma_{\gamma e} \approx \frac{3}{8}\frac{\sigma_{\rm Th}}{\omega}\left[\ln 2\omega + \frac{1}{2} + {\rm O}\left(\frac{\ln\omega}{\omega}\right)\right] \qquad \omega \gg 1, \tag{D12}$$

where $\omega \equiv E_\gamma/m_e$ and $\sigma_{\rm Th}$ is the Thomson cross section. The cumulative probability distribution that the γ scatters to energy $E'_\gamma \le E^c_\gamma$ during the Compton scattering process may be derived by utilizing the results in Ref. [53] and is found as

$$P_c(E_\gamma, E'_\gamma \le E^c_\gamma) \approx \frac{\frac{1}{2}x^2 - \ln\frac{1}{x} + \ln 2\omega}{\frac{1}{2} + \ln 2\omega} + {\rm O}(1/\omega), \tag{D13}$$

where $x \equiv E^c_\gamma/E_\gamma$ and the kinematic limits of x fall in the range 1 and $1/(1 + 2\omega) \approx 1/2\omega$. The scattered electrons may produce further γ rays by inverse Compton scattering on the CMBR, an effect which is taken into account in the calculations.

d. γ-γ scattering

Following the analysis of Svensson and Zdziarski [49,50], the total rate for scattering of a γ ray of energy E_γ on a blackbody of temperature T is given by

$$R_{\gamma\gamma} = \frac{2^4 139\pi^3}{3^6 5^4}\alpha^4 m_e \left(\frac{T}{m_e}\right)^6 \left(\frac{E_\gamma}{m_e}\right)^3. \tag{D14}$$

Employing Eq. (3.9) of Ref. [50], one may compute the cumulative probability distribution for the energy of the scattered photon E'_γ to be below E^c_γ as

$$P_c(E_\gamma, E'_\gamma \le E^c_\gamma) = \frac{10}{7}x\left[1 - x + x^2 - \frac{1}{2}x^3 + \frac{1}{5}x^4\right], \tag{D15}$$

where $x \equiv E^c_\gamma/E_\gamma \le 1$. The energy of the scattered blackbody photon is given approximately by $E'_{\gamma,BB} \approx E_\gamma - E'_\gamma$ in the limit $T \ll E_\gamma$ and its effects are treated in the calculations as well.

3. Photodisintegration

Photodisintegration of the light elements by γ rays generated as a consequence of relic particle decays plays a particularly important role in the determination of BBN yields, as noted early on [12]. It is only effective at temperatures below $T \lesssim 6$ keV (cf. Fig. 5), since at higher temperatures γ rays of sufficient energy $E_g \approx 2$ MeV to photodisintegrate ^{2}H, ^{7}Li, and ^{7}Be predominantly pair produce on the abundant CMBR photons (cf. Appendix D 2). Below this approximate cosmic temperature, pair production is kinematically forbidden such that photodisintgeration becomes probable. The competing Bethe-Heitler pair production, Compton scattering, and $\gamma\gamma$ scattering were described in the previous subsections.

The (lowest) photodisintegration thresholds for the various light nuclei synthesized during BBN ^{2}H, ^{3}H, ^{3}He, ^{4}He, ^{6}Li, ^{7}Li, and ^{7}Be are given by 2.225 MeV, 6.257 MeV, 5.493 MeV, 19.814 MeV, 3.699 MeV, 2.467 MeV, and 1.587 MeV, respectively. The present analysis utilizes photodisintegration data as parametrized by Ref. [19] with a few of these parametrizations changed to produce improved fits to the available reaction data. For original references the reader is referred to the references in Ref. [19].

In addition, the reactions 23–26, and 30–33, not considered in Ref. [19], have been included in the present analysis. Here the following parametrizations of reaction rate data [54–56] have been adopted:

reaction 23 [54]
$$\sigma(E_\gamma) = 3.8\ {\rm mb} Q_0^{2.3}(E_\gamma - Q_0)/E_\gamma^{3.3} + (2.1\ {\rm mb} Q_1^{1.5}(E_\gamma - Q_1)/E_\gamma^{2.5}) \times \Theta(E - Q_1), \tag{D16}$$
with $Q_0 = 8.725$ MeV and $Q_1 = 23$ MeV and $\Theta(x)$ the step function;

reaction 24 [54,55]
$$\sigma(E_\gamma) = 10.8\ {\rm mb} Q^2 \times (E_\gamma - Q)^{1.2}/E_\gamma^{3.2}, \tag{D17}$$
with $Q = 9.98$ MeV; and

reaction 25 [56]
$$\sigma(E_\gamma) = 1.44 \times 10^3\ {\rm mb} Q^{20} \times (E_\gamma - Q)^{2.4}/E_\gamma^{22.4}, \tag{D18}$$
with $Q = 22.28$ MeV.

Reaction 26 has been parametrized as reaction 25 but with $Q = 23.05$ MeV since no experimental data exists. Similarly, since no reaction rate data exists for the cross sections of reactions 30–33, they have been approximated by the data of their respective mirror reactions 23–26 but with binding energies appropriately replaced by, $Q = 7.08$ MeV, $Q = 10.68$ MeV, $Q = 22.17$ MeV, and $Q = 21.40$ MeV for reactions 30,31,32, and 33, respectively.

APPENDIX E: NONTHERMAL HADRONIC INTERACTIONS

1. Mesonic induced charge-exchange reactions

Injection of mesons in the form of metastable pions and kaons may induce the charge-exchange reactions 34–43 to convert protons to neutrons and vice versa [15]. As essentially each neutron is incorporated into a helium nuclei at $T \approx 80$ keV, mesons may thus effect the ^{4}He abundance. Since more protons are converted to neutrons than vice versa, injection of mesons leads to an increase in the ^{4}He abundance. Mesonic charge-exchange reactions are particularly important at fairly high temperatures. At $T \approx 1$ MeV, for example, a fraction ~ 0.01 of all mesons induce charge exchange with the remainder decaying. In contrast, this fraction drops to $\sim 10^{-5}$ at $T \approx 100$ keV. The present analysis follows the treatment of Ref. [15] and the reader is referred to this study for details.

The mesons may be due to a variety of processes. It is well known that the hadronic decay (or annihilation) results in a multitude of mesons. However, under certain circumstances even electromagnetic and weak decays may yield mesons. This may be due to decays involving $\tau^{\pm}$ in the final state, which have a branching ratio to pions. Similarly injection of high-energy $E_\nu \sim 100$ GeV neutrinos at $T \sim 1$ MeV may pair produce $\pi^{\pm}$ on the neutrino background. Pair production of pions by γ scattering on the CMBR [21] is unlikely as the Compton cross section is typically a factor ~ 300 larger.

Production of mesons by electromagnetically or weakly interacting particles has not been included in the present study. In the case of hadronic decays their effect is subdominant, and in the case of electromagnetic and weak decays the analysis is model dependent on the decay products.

2. Nucleon-antinucleon annihilations

Hadronic decays lead to the production of nucleons and antinucleons. It is assumed here that the total baryon number is conserved during the decay. At higher temperatures ($T \gtrsim 90$ keV for n and $\bar{n}$ and $T \gtrsim 20$ keV for p and $\bar{p}$) they thermalize by electromagnetic energy losses (cf. Appendix D 1) with antinucleons annihilating at rest thereafter. The combination of injection of nucleons (with a predefined n/p ratio, typically close to 1) and annihilation of antinucleons on the preexisting nucleons may lead to an increase of the neutron-to-proton ratio and the ^{4}He abundance resulting from BBN [15]. Antinucleons mostly annihilate on protons due to the small thermal n/p ratio and due to Coulomb enhancement of the $\bar{p}p$ annihilation cross section. The annihilated protons are replaced by the injected nucleons which typically come in a ratio $n/p \approx 1$ thus yielding an effective increase of the n/p ratio. Given a typical injected meson-to-(anti-)baryon ratio of ~ 20 in hadronic decays, the effects of nucleon antinucleon injection are far more important than those of mesonic charge-exchange reactions. This holds particularly true at lower temperatures $T \lesssim 300$ keV. The present study uses the reaction rate data as given in Ref. [15].

When electromagnetic stopping becomes less dominant at lower temperatures, thermalization of energetic nucleons occurs partially due to nucleon-nucleon scattering and nuclear spallation (cf. Appendices E 3–E 5). Antinucleons, on the other hand, never thermalize but rather annihilate during one of their first interactions with thermal protons or helium nuclei. As an energetic nucleon has of the order of ~ 20 N-N scattering events before dropping below the ^{4}He spallation threshold, its probability to inflict a ^{4}He spallation event is factor ~ 10 larger than that of an antinucleon. It has been therefore approximated that antinucleons do never spall ^{4}He, leading to about a 10% underestimate in ^{2}H, ^{3}H, and ^{3}He production due to particle decay.

3. Elastic N-N scattering

Elastic nucleon-nucleon scattering and nucleon-^{4}He scattering of energetic neutrons and protons off the thermal protons and ^{4}He is important in the nucleon thermalization process, in particular, at lower temperature ($T \lesssim 90$ keV for n's and $T \lesssim 20$ keV for p's) and when the nucleons are not too energetic, i.e. $E \lesssim 1$ GeV. This may be seen in Fig. 1. In contrast, very energetic nucleons, $E \gg 1$ GeV, are stopped at lower temperatures mostly by inelastic scatterings of protons and ^{4}He (cf. Appendices E 4 and E 5) and at higher temperatures either by Thomson scattering off CMBR photons in the case of protons (cf. Appendix D 1 b) or magnetic moment scatterings off thermal $e^{\pm}$ in the case of neutrons (cf. Appendix D 1 c). Elastic scatterings off protons also produce secondary energetic protons which are taken into account in the present study.

For the elastic p-p, n-p, p-^{4}He, and n-^{4}He scattering cross sections we take the data as compiled by Ref. [25]. This compilation compares well with that given in the more recent compilation given in Ref. [33]. It is noted here that due to approximate isospin invariance the p-^{4}He, and n-^{4}He cross sections are almost equal. To calculate the energy loss in p-p and n-p scattering events, an against nuclear data tested algorithm presented in Ref. [26] is used. Each scattering event is treated by a Monte Carlo. This algorithm predicts an almost uniform probability distribution for fractional energy loss $\Delta E_k/E_k$ for $\lesssim 250$ MeV protons progressing smoothly towards a bimodal probability distribution (either forward scattering, i.e. $\Delta E_k/E_k \approx 0$ or backward scattering, i.e. $\Delta E_k/E_k \approx 1$) when the p kinetic energy is increased towards 2 GeV. Neutron-proton scattering follows a similar though less well-defined trend. For kinetic energies $E_k > 2$ GeV, the probability distributions of 2 GeV nucleons are utilized.

Nucleon-^{4}He scattering follows a very different pattern with ^{4}He recoil energies to high probability very small. Given data by Ref. [57], the typical ^{4}He recoil energy is

approximated at 5 MeV in each event. It has been verified that a change in this recoil energy has negligible effect on the BBN yields. For a more detailed discussion on the ^{4}He recoil energies which play a role in ^{4}He–^{4}He fusion reactions 87 and 88, the reader is referred to Appendix E 6.

4. Inelastic *N*-*N* scattering

For nucleon-nucleon scattering with nucleon kinetic energies in the GeV range, scattering processes are mostly inelastic accompanied by the production of pions. Treating these processes properly is important not only for a determination of the typical nucleon energy loss, but also because scattering processes may easily convert protons to neutrons and vice versa. In fact, due to a large asymmetry in the cross sections the conversion of energetic protons to neutrons occurs more often than the inverse of this process. This has implication for spallation processes, increasing ^{2}H, ^{3}H, ^{3}He, and ^{6}Li yields, as neutrons are stopped by scattering off protons and ^{4}He for temperatures $T \lesssim 90$ keV, whereas $E_p \lesssim 1$ GeV protons mostly lose their energy via Coulomb stopping. This study uses the inelastic *N*-*N* cross sections reactions 52–73 in Table I as compiled by Ref. [24], where some of the proposed fitting functions had to be modified by the author to correctly account for the data. Concerning the total average energy loss f_π into pion mass and kinetic energy in inelastic scatterings, experimental data by Ref. [58] at $E_p = 790$ MeV and a simulation with PYTHIA at $E_p = 53$ GeV has been fitted logarithmically to obtain $f_\pi \approx 0.2 + 0.08 \ln(E/0.8\ \mathrm{GeV})$. The remainder of the energy has been split in proportions (0.15,0.85) between the outgoing nucleons roughly equal to the average energy split for energetic elastic collisions. For the nucleon energy loss in the inelastic spallation processes discussed in Appendix E 5, it has been assumed that the outgoing nucleons are missing the binding energy necessary for the spallation process, and the remaining energy is shared between primary and secondary nucleon in proportion (0.75,0.25). This corresponds to the average values for elastic *N*-*N* scattering in the several hundred of MeV range.

5. Nuclear spallation

Aside from ^{4}He photodisintegration which is operative only at lower cosmic temperatures $T \lesssim 3$ keV, ^{4}He spallation reactions at temperatures $T \lesssim 90$ keV induced by energetic nucleons are the main source of additional ^{2}H, ^{3}H, ^{3}He, as well as ^{6}Li (through nonthermal fusion reactions induced by energetic mass three nuclei, cf. Appendix E 6) in BBN with decaying particles. It is therefore important to employ accurate reaction cross section data. The ^{4}He-spallation reactions 74–83 in Table I have been included in the analysis. Experimental data on these reactions has been obtained at nucleon energies $E =$ 28 MeV [59], 53 MeV [60], 90 MeV [61], 220 MeV [62], 300 MeV [63], 620 MeV [64], 1.42 GeV [65], and 2.61 GeV [65], respectively, and has been interpolated in between. This data and the interpolation is shown in Fig. 11. The data also includes the possible production of additional pions in the spallation process. Note that ^{4}He-spallation data induced by either neutrons or protons has been included on an equal basis in the compilation. Here reactions induced by neutrons, such as $^4\mathrm{He}(n, np)^3\mathrm{H}$, have been associated with their corresponding mirror reactions induced by protons, i.e. $^4\mathrm{He}(p, np)^3\mathrm{He}$. This is theoretically and experimentally justified due to approximate isospin invariance, as long as Coulomb effects are negligible, in particular, for nucleon energies larger than a few MeV. For the energies of nucleons and nuclei after the spallation, the reader is referred to Appendices E 4 and E 6. The spallation of energetic freshly synthesized ^{6}Li reaction 84 also has been included [66] but plays only a minor role for the results.

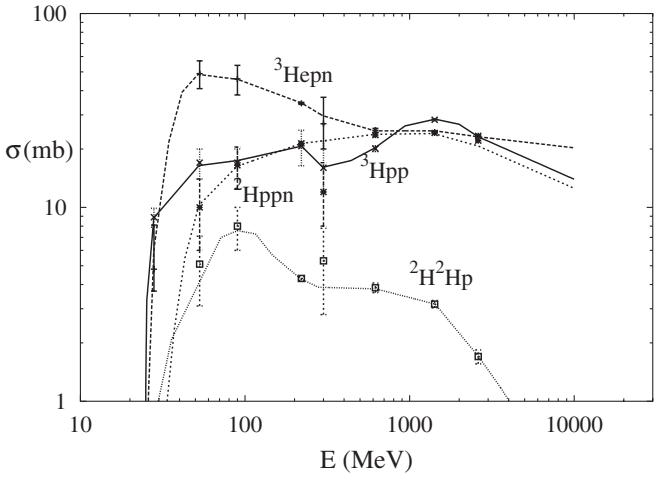

FIG. 11. Compilation of the available ^{4}He spallation data as a function of nucleon kinetic energy (with ^{4}He at rest) for the spallation reactions 74, 75, 76, and 78. The lines joining independent data points (74, solid line; 75, long dashed line; 76, short dashed line; 78, dotted line) represent the fit used in the present analysis. Refer to the text for references.

6. Nonthermal fusion reactions

Nonthermal fusion reactions are particularly important for the formation of ^{6}Li, which during thermal BBN is produced only in very small amounts. When relic particles decay during or after BBN, ^{6}Li is therefore the first element which becomes significantly perturbed compared to its SBBN abundance. This has been shown first in the case of hadronic decays in Ref. [14] and later in the case of electromagnetic decays in Ref. [17]. The most efficient reaction sequence is initiated by either the spallation $^4\mathrm{He}(N, \ldots$ or photodisintegration $^4\mathrm{He}(\gamma, \ldots$ of ^{4}He to produce energetic ^{3}H and ^{3}He nuclei. These later may then fuse on ambient ^{4}He nuclei to form ^{6}Li via $^3\mathrm{H}(^4\mathrm{He}, n)^6\mathrm{Li}$ and $^3\mathrm{He}(^4\mathrm{He}, p)^6\mathrm{Li}$. If only a small fraction $\sim 10^{-4}$ (cf. Fig. 2) of these energetic mass three nuclei fuse, an observationally important ^{6}Li abundance may result.

Energetic mass three nuclei in the tens of MeV range are essentially all stopped by Coulomb interactions. Since this process is less efficient at higher energy [i.e. $(1/E_3)dE_3/dx \propto E_3^{-2}$; cf. Appendix D 1 a] and since the fusion cross section does not drastically fall with energy, the formation of ^{6}Li is very sensitive towards the high-energy tail of produced mass three nuclei. It will be seen that the lack of knowledge of this tail actually introduces some uncertainty in the ^{6}Li yield.

In this paper the ^{3}H(^{4}He, n)^{6}Li and ^{3}He(^{4}He, p)^{6}Li cross sections as determined with the aid of reverse reaction rate data by Ref. [67] and Ref. [19], respectively, have been adopted. Here the first reaction has a threshold in the ^{4}He rest frame of $E_{\rm th} = 8.39$ MeV, whereas the second reaction has $E_{\rm th} = 7.05$ MeV. Cross sections for the spallation and photodisintegration reactions are taken as described in Appendices D 3 and E 5, respectively. Concerning the ''recoil'' energy distributions of the mass three nuclei in the case of photodisintegration, it is given by $E_3 = (E_\gamma - E_{\gamma,\rm th}^{^4\rm He})m_N/(m_N + m_3)$ for ^{3}H nuclei, whereas for spallation one has to resort to experimental data. Data has been published for the ^{4}He(n, np)^{3}H reaction [61] at $E_n = 90$ MeV in the ^{4}He rest frame and more recently for the ^{4}He(p, pp)^{3}H and ^{4}He(p, np)^{3}He reactions [68] at $E_p = 220$ MeV. Data at higher energies exists as well [69] which lies above the threshold of pion production during the spallation process. In general, the energy distributions of mass three nuclei seem almost independent of incident nucleon energy though care has to be taken in the comparison since sometimes only partial (quasifree-scattering) distributions are shown (as in the case of Ref. [69]). In this study the complete distributions as given in Ref. [68] are utilized (in binned form) for both the ^{4}He($p, \ldots$ reactions and their ^{4}He($n, \ldots$ corresponding mirror reactions. The utilization of reaction rate data of the corresponding mirror reactions seems not only theoretically justified [25,70] but also when experimental data of Refs. [61,68] are directly compared.

Some uncertainty in the ^{6}Li yield results from an inaccurate determination of the few percent high-energy tail in the mass three nuclei energy distribution function. The highest energy events are particularly difficult to detect in bubble chamber experiments [70], such that the distribution of Ref. [68] only extends towards $E_3 \approx 90$ MeV. In Ref. [61] a fraction of about 2% of all spallation reactions seem to result in ^{3}H nuclei at the kinematically highest allowed energy. This corresponds to backward scattering and such peaks in the distribution functions are also observed in ^{4}He-^{4}He elastic scatterings [71]. If the four-event backward scattering peak as observed in Ref. [61] is real, rather than a fluctuation or measurement error, resulting ^{6}Li yields may increase by some tens of percents due to these high-energy mass three nuclei (cf. Fig. 2). However, on conservative grounds, this study neglects ^{6}Li production due to the very highest energy mass three nuclei.

Energetic mass three nuclei may also be produced by ^{4}He($n, ^2$H)^{3}H and its mirror reaction. For the energy distributions of this subdominant mass three nuclei channel reaction, data of the compilation/determination in Refs. [25,72] at proton kinetic energies of 55 MeV, 85 MeV, and 156 MeV, respectively, have been interpolated. Fusion reactions such as ^{2}H(α, γ)^{6}Li, ^{3}H(α, γ)^{7}Li, and ^{3}He(α, γ)^{7}Be have not been considered as cross sections involving the emission of a photon are typically only in the nb to μb range. The $N(N, \pi' s)^2$H reaction, on the other hand, is treated as discussed in Appendix E 4.

Note that in a narrow temperature interval around $T \sim$ 3–20 keV Coulomb stopping of not too energetic $E_3 \sim$ 10–30 MeV mass three nuclei loses its efficiency (cf. Appendix D 1 a) due to the nuclei velocity falling below a typical electron thermal velocity. In this regime of efficient ^{6}Li synthesis, other processes reactions 89–91 which contribute to the thermalization of mass three nuclei may become of some limited importance. They have been included in the calculation by taking data from Ref. [73]. At very low temperatures $T \lesssim 1$ eV energetic ^{3}H stopping times may become longer than the ^{3}H decay time. It is therefore possible that ^{3}H decays to ^{3}He before it falls below the ^{6}Li fusion threshold and this effect has been taken into account.

Fusion reaction between energetic ^{4}He (produced by N-^{4}He elastic scatterings) and thermal ^{4}He nuclei may, in principle, also lead to the synthesis of ^{6}Li, as well as ^{7}Li. In practice, however, this process is subdominant and has therefore not been included. The threshold energies for ^{4}He(α, p)^{7}Li and ^{4}He(α, pn)^{6}Li are 37.8 MeV and 49.2 MeV, respectively. These are much larger than those for the fusion of mass three nuclei on ^{4}He. Given the data in Ref. [57], the distribution function for recoil energies of ^{4}He nuclei in N-^{4}He elastic scattering may be approximated by an exponential distribution $dP/dE_4 \approx a\exp(-bE_4)$ with $a \approx 225$ mb/GeV and $b \approx 65$ GeV^{-1}, independent of nucleon kinetic energy. The total cross section for producing $E_4 \gtrsim 50$ MeV recoil ^{4}He in N-^{4}He scatterings is thus in the $\sim$0.1 mb range. Note that $E_4 \gtrsim 50$ MeV has been chosen as only for such energies as the ^{4}He-^{4}He fusion cross section becomes appreciable $\sim$100 mb [74]. The cross section of $\sim$0.1 mb for the production of ^{4}He nuclei energetic enough to produce ^{6}Li by fusion has to be compared to the typical total cross sections for ^{4}He($N, \ldots$)^{3}H, etc. of $\sim$30 mb times the fraction $\sim$0.3 of mass three nuclei energetic enough to fuse to ^{6}Li. This yields $\sim$10 mb compared to 0.1 mb. Nevertheless, ^{6}Li fusion via ^{4}He nuclei is enhanced due to a less efficient Coulomb stopping at 50 MeV versus the canonical 10 MeV for mass three nuclei, resulting in an enhancement factor of $(50/10)^2/4 \approx 6$. Here the 4 in the denominator comes from the factor two higher charge of ^{4}He nuclei compared to ^{3}H nuclei. Altogether it is found that energetic ^{4}He

contributes only of the order ~6% to the final ^{6}Li abundance This is also not changed by the existence of a sharp backward scattering peak in N-^{4}He scattering [71] which, similarly to the possible existence of a backward peak in the mass three nuclei distribution (see above) may increase the ^{6}Li synthesis due to energetic ^{4}He by a factor ~1.2.

APPENDIX F: THERMAL NUCLEAR REACTIONS

Thermal nuclear reactions are treated by the Kawano code updated by the NACRE [75] reaction compilation. For the neutron life time the value $\tau_n = 885.7$ sec is used as quoted as the ''world'' average in the Particle Data Booklet. For the fractional contribution of baryons to the critical density the central value as determined by three years of WMAP observations [2] $\Omega_b h^2 = 0.02233^{+0.072}_{-0.091}$ is applied. Given the conversion $\Omega_b h^2 = 3.65 \times 10^7 \eta$ this corresponds to a baryon-to-photon ratio of $\eta = n_b/n_\gamma = 6.12 \times 10^{-10}$. With these input values the abundances within a SBBN scenario are found at $^2\mathrm{H/H} = 2.68 \times 10^{-5}$, $^3\mathrm{He}/^2\mathrm{H} = 0.38$ ($^3\mathrm{He/H} = 1.04 \times 10^{-5}$) $Y_p = 0.248$, and $^7\mathrm{Li/H} = 4.34 \times 10^{-10}$, respectively. The ^{6}Li abundance in a SBBN scenario is negligible compared to the observationally inferred value of ^{6}Li in low-metallicity stars.

[1] R. A. Malaney and G. J. Mathews, Phys. Rep. **229**, 145 (1993); S. Sarkar, Rep. Prog. Phys. **59**, 1493 (1996); K. Jedamzik, astro-ph/9805156; H. Kurki-Suonio, astro-ph/0002071.
[2] D. N. Spergel *et al.*, astro-ph/0603449.
[3] M. H. Pinsonneault, T. P. Walker, G. Steigman, and V. K. Narayanan, Astrophys. J. **527**, 180 (1999).
[4] O. Richard, G. Michaud, and J. Richer, Astrophys. J. **619**, 538 (2005).
[5] M. Salaris and A. Weiss, Astron. Astrophys. **376**, 955 (2001).
[6] S. Theado and S. Vauclair, Astron. Astrophys. **375**, 70 (2001).
[7] L. Piau, T. C. Beers, D. S. Balsara, T. Sivarani, J. W. Truran, and J. W. Ferguson, astro-ph/0603553.
[8] K. Jedamzik, Phys. Rev. D **70**, 063524 (2004).
[9] K. Jedamzik, K. Y. Choi, L. Roszkowski, and R. Ruiz de Austri, J. Cosmol. Astropart. Phys. 07 (2006) 007.
[10] S. Weinberg, Phys. Rev. Lett. **48**, 1303 (1982); H. Pagels and J. R. Primack, Phys. Rev. Lett. **48**, 223 (1982); M. Y. Khlopov and A. D. Linde, Phys. Lett. **138B**, 265 (1984).
[11] F. Balestra *et al.*, Lett. Nuovo Cimento Soc. Ital. Fis. **41**, 223 (1984).
[12] D. Lindley, Astrophys. J. **294**, 1 (1985).
[13] J. Ellis, D. Nanopoulos, and S. Sarkar, Nucl. Phys. **B259**, 175 (1985); R. Juszkiewicz, J. Silk, and A. Stebbins, Phys. Lett. **158B**, 463 (1985); Audouze, D. Lindley, and J. Silk, Astrophys. J. **293**, L53 (1985); D. Lindley, Phys. Lett. B **171**, 235 (1986); M. Kawasaki and K. Sato, Phys. Lett. B **189**, 23 (1987); R. J. Scherrer and M. S. Turner, Astrophys. J. **331**, 19 (1988); Y. L. Levitan, I. M. Sobol, M. Y. Khlopov, and V. M. Chechetkin, Sov. J. Nucl. Phys. **47**, 109 (1988).
[14] S. Dimopoulos, R. Esmailzadeh, L. J. Hall, and G. D. Starkman, Astrophys. J. **330**, 545 (1988); Nucl. Phys. **B311**, 699 (1989).
[15] M. H. Reno and D. Seckel, Phys. Rev. D **37**, 3441 (1988).
[16] J. R. Ellis, G. B. Gelmini, J. L. Lopez, D. V. Nanopoulos, and S. Sarkar, Nucl. Phys. **B373**, 399 (1992); Kawasaki and T. Moroi, Prog. Theor. Phys. **93**, 879 (1995); J. Protheroe, T. Stanev, and V. S. Berezinsky, Phys. Rev. D **51**, 4134 (1995); M. Yu. Khlopov, Yu. L. Levitan, E. V. Sedelnikov, and I. M. Sobol, Phys. At. Nucl. **57**, 1393 (1994); E. V. Sedelnikov, S. S. Filippov, and M. Y. Khlopov, Phys. At. Nucl. **58**, 235 (1995); E. Holtmann, M. Kawasaki, K. Kohri, and T. Moroi, Phys. Rev. D **60**, 023506 (1999).
[17] K. Jedamzik, Phys. Rev. Lett. **84**, 3248 (2000).
[18] M. Kawasaki, K. Kohri, and T. Moroi, Phys. Rev. D **63**, 103502 (2001); K. Kohri, Phys. Rev. D **64**, 043515 (2001).
[19] R. H. Cyburt, J. R. Ellis, B. D. Fields, and K. A. Olive, Phys. Rev. D **67**, 103521 (2003).
[20] M. Kawasaki, K. Kohri, and T. Moroi, Phys. Lett. B **625**, 7 (2005).
[21] M. Kawasaki, K. Kohri, and T. Moroi, Phys. Rev. D **71**, 083502 (2005).
[22] K. Jedamzik, Phys. Rev. D **70**, 083510 (2004).
[23] D. G. Cerdeno, K. Y. Choi, K. Jedamzik, L. Roszkowski, and R. Ruiz de Austri, J. Cosmol. Astropart. Phys. 06 (2006) 005.
[24] J. Bystricky, P. La France, F. Lehar, F. Perrot, T. Siemiarczuk, and P. Winternitz, J. Phys. (France) **48**, 1901 (1987).
[25] J. P. Meyer, Astron. Astrophys. Suppl. Ser. **7**, 417 (1972).
[26] R. A. Arndt, I. I. Strakovsky, and R. L. Workman, Int. J. Mod. Phys. A **18**, 449 (2003); Fortran program SAID for the calculation of nucleon-nucleon amplitudes, http://gwdac.phys.gwu.edu, with courtesy provided by Dick Arndt.
[27] An own fit to the data has been used since the fit as proposed by Ref. [24] is not adequate.
[28] Cross section approximated by the parametrization given in Ref. [19] after comparison with published data in the Experimental Nuclear Reaction Data Base (EXFOR). For the original references the reader is referred to the EXFOR database and Ref. [19].
[29] Prefactor in the parametrizations of this reaction in Ref. [19] changed from 17.1 mb to 20.7 mb to account for EXFOR data.
[30] Prefactor in Ref. [19] changed from 104 mb to 143 mb to account for EXFOR data.
[31] The parametrization as given in Ref. [19] is adopted. Nevertheless, when reverse reaction rate data from NACRE [75] is used to evaluate the cross section, the

parametrization leads to a factor 2–3 overestimate of the cross section. In contrast, when direct reaction data assembled by Ref. [54] is used, the parametrization leads to a factor 2–3 underestimate of the cross section. Other direct reaction rate data, such as of Ref. [76], also does not lead to a favorable comparison. It is concluded that the adopted ^{7}Li(γ, ^{3}H)^{4}He cross section has large uncertainties. Since constraints from ^{7}Li are rather weak, this has only little impact on the presented constraints.

[32] The parametrization of Ref. [19] is adopted with nevertheless negative values of σ which occur at larger E_γ in this parametrization set to zero. Direct reaction data for this reaction does not exist. As in the case of the reaction ^{7}Li(γ, ^{3}H)^{4}He, an evaluation of the cross section by the author utilizing reverse reaction rate data from Ref. [75] indicates a possible overestimate of the cross section as parametrized in Ref. [19]. Nevertheless, as constraints from other light elements are more stringent, this possible overestimate has only negligible influence on the conclusions.

[33] S. Eidelmann *et al.*, Phys. Lett. B **592**, 1 (2004); http://pdg.lbl.gov/.

[34] M. Asplund, D. L. Lambert, P. E. Nissen, F. Primas, and V. V. Smith, Astrophys. J. **644**, 229 (2006).

[35] M. Pospelov, hep-ph/0605215; K. Kohri and F. Takayama, hep-ph/0605243; R. H. Cyburt, J. Ellis, B. D. Fields, K. A. Olive, and V. C. Spanos, astro-ph/0608562; M. Kaplinghat and A. Rajaraman, astro-ph/0606209.

[36] G. Steigman, Int. J. Mod. Phys. E **15**, 1 (2006).

[37] B. Fields and S. Sarkar, astro-ph/0601514.

[38] Y. I. Izotov and T. X. Thuan, Astrophys. J. **602**, 200 (2004).

[39] V. Luridiana, A. Peimbert, M. Peimbert, and M. Cervino, Astrophys. J. **592**, 846 (2003).

[40] K. A. Olive and E. D. Skillman, Astrophys. J. **617**, 29 (2004).

[41] J. M. O'Meara, D. Tytler, D. Kirkman, N. Suzuki, J. X. Prochaska, D. Lubin, and A. M. Wolfe, Astrophys. J. **552**, 718 (2001); M. Pettini and D. V. Bowen, Astrophys. J. **560**, 41 (2001); D. Kirkman, D. Tytler, N. Suzuki, J. M. O'Meara, and D. Lubin, Astrophys. J. Suppl. Ser. **149**, 1 (2003); N. H. M. Crighton, J. K. Webb, A. Ortiz-Gill, and A. Fernandez-Soto, Mon. Not. R. Astron. Soc. **355**, 1042 (2004).

[42] G. Sigl, K. Jedamzik, D. N. Schramm, and V. S. Berezinsky, Phys. Rev. D **52**, 6682 (1995).

[43] G. Gloeckler and J. Geiss, *Light Elements and Their Evolution, Proceedings of the IAU Symposia 198, Natal, Brazil, 1999* (IAU, Natal, Brasil, 2000), p. 224.

[44] P. Bonifacio and P. Molaro, Mon. Not. R. Astron. Soc. **285**, 847 (1997).

[45] S. G. Ryan, J. E. Norris, and T. C. Beers, Astrophys. J. **523**, 654 (1999).

[46] V. V. Smith, D. L. Lambert, and P. E. Nissen, Astrophys. J. **408**, 262 (1993); **506**, 405 (1998); R. Cayrel, M. Spite, F. Spite, E. Vangioni-Flam, M. Cassé, and J. Audouze, Astron. Astrophys. **343**, 923 (1999); P. E. Nissen, M. Asplund, V. Hill, and S. D'Odorico, Astron. Astrophys. **357**, L49 (2000).

[47] J. D. Jackson, in *Classical Electrodynamics* (Wiley, New York, 1999).

[48] F. A. Aharonian, V. G. Kirillov-Ugryumov, and V. V. Vardanian, Astrophys. Space Sci. **115**, 201 (1985).

[49] A. A. Zdziarski and R. Svensson, Astrophys. J. **344**, 551 (1989).

[50] R. Svensson and A. A. Zdziarski, Astrophys. J. **349**, 415 (1990).

[51] R. J. Protheroe, T. Stanev, and V. S. Berezinsky, Phys. Rev. D **51**, 4134 (1995).

[52] M. Kawasaki and T. Moroi, Astrophys. J. **452**, 506 (1995).

[53] C. Itzykson and J.-P. Zuber, in *Quantum Field Theory* (McGraw-Hill Book Company, New York, 1980).

[54] V. V. Varlamov *et al.*, Report No. B,CDFE/LI2, 1986.

[55] Yu. M. Volkov *et al.*, Zhurnal Eksperimental'noi Teoret. Fiziki, Russia **42**, 108 (1962); V. P. Denisov *et al.*, Yadernaya Fizika **5**, 490 (1967).

[56] E. A. Kotikov *et al.*, Yadernaya Fizika **46**, 1009 (1987).

[57] L. G. Votta *et al.*, Phys. Rev. C **10**, 520 (1974); V. Comparat *et al.*, Phys. Rev. C **12**, 251 (1975); R. Klem *et al.*, Phys. Lett. **70B**, 155 (1977); V. V. Glagolev *et al.*, Phys. Rev. C **18**, 1382 (1978).

[58] W. Thomas *et al.*, Phys. Rev. D **24**, 1736 (1981).

[59] A. F. Wickersham, Phys. Rev. **107**, 1050 (1957).

[60] D. J. Cairns *et al.*, Nucl. Phys. **60**, 369 (1964).

[61] P. E. Tannenwald, Phys. Rev. **89**, 508 (1953).

[62] S. K. Abdullin *et al.*, Nucl. Phys. **A569**, 753 (1994).

[63] W. H. Innes, University of California Radiation Laboratory Report No. UCRL-8040.

[64] A. V. Blinov *et al.*, Phys. At. Nucl. **64**, 907 (2001).

[65] V. V. Glagolev *et al.*, Z. Phys. C **60**, 421 (1993).

[66] A. J. Elwyn *et al.*, Phys. Rev. C **20**, 1984 (1979).

[67] E. Sihvola, Phys. Rev. D **63**, 103001 (2001).

[68] A. V. Blinov *et al.*, Phys. At. Nucl. **58**, 1713 (1995).

[69] V. V. Glagolev *et al.*, Phys. Rev. C **18**, 1382 (1978); A. Dirner *et al.*, Eur. Phys. J. A **8**, 493 (2000).

[70] Marina Chadeyeva (private communication).

[71] J. Berger *et al.*, Phys. Rev. Lett. **41**, 152 (1978).

[72] L. G. Votta *et al.*, Phys. Rev. C **10**, 520 (1974).

[73] B. Haesner *et al.*, Phys. Rev. C **28**, 995 (1983).

[74] B. G. Glagola *et al.*, Phys. Rev. Lett. **41**, 1698 (1978); D. J. Mercer *et al.*, Phys. Rev. C **63**, 065805 (2001).

[75] C. Angulo *et al.*, Nucl. Phys. **A656**, 3 (1999).

[76] G. M. Griffiths *et al.*, Can. J. Phys. **39**, 1397 (1961).